UHASSELT
KNOWLEDGE IN ACTION

Maastricht University

Faculty of Medicine and Life Sciences
School for Life Sciences
Master of Biomedical Sciences

Masterthesis

Development of a polymer resin as an improved adhesion layer in molecularly imprinted polymer based biosensors

Emma Van de Reydt

Thesis presented in fulfillment of the requirements for the degree of Master of Biomedical Sciences, specialization Bioelectronics and Nanotechnology

SUPERVISOR :
Prof. dr. Tanja JUNKERS

CO-SUPERVISOR :
Prof. dr. ir. Ronald THOELEN

MENTOR :
De heer Gijs RAMAKERS

2017
2018

Transnational University Limburg is a unique collaboration of two universities in two countries: the University of Hasselt and Maastricht University.

UHASSELT
KNOWLEDGE IN ACTION

www.uhasselt.be
Universiteit Hasselt
Campus Hasselt:
Martelarenlaan 42 | 3500 Hasselt
Campus Diepenbeek:
Agoralaan Gebouw D | 3590 Diepenbeek

Maastricht University

Faculty of Medicine and Life Sciences
School for Life Sciences
Master of Biomedical Sciences

Masterthesis

Development of a polymer resin as an improved adhesion layer in molecularly imprinted polymer based biosensors

Emma Van de Reydt

Thesis presented in fulfillment of the requirements for the degree of Master of Biomedical Sciences, specialization Bioelectronics and Nanotechnology

SUPERVISOR :
Prof. dr. Tanja JUNKERS

CO-SUPERVISOR :
Prof. dr. ir. Ronald THOELEN

MENTOR :
De heer Gijs RAMAKERS

Foreword and acknowledgements

First and foremost, I would like to thank Prof. Dr. Tanja Junkers for giving me the opportunity to work on this project and giving me the opportunity to discover chemistry as tool to solve biomedical related problems. I would also like to thank Prof. Ir. Dr. Ronald Thoelen since without his collaboration, this project wouldn't even exist. For the midterm evaluation, I would like to thank Prof. Dr. Milos Nesladek, who showed genuine interest in the project.

Furthermore, my daily supervisor and mentor Gijs Ramakers deserves special thanks for his patience, and willingness to help wherever possible. Working on this thesis would not be the same without his guidance. I would like to express my very great appreciation to the whole PRD group, all people who not only provided advice and wisdom but also accepted me as part of the group. I'm grateful for the help from Lowie Maes and Jeroen De Neve, who were willing to measure the ESI-MS spectra of my samples. For letting me borrow a part of her hood and helping me with the flow experiments, special thanks goes to Erika Mertens. Dr. Joachim Laun deserves special credit since he is the one who convinced me to discover the world of chemistry with his enthusiastic teaching during the junior stage. I'd like to thank Frederik Vreys and Thijs Vandenryt for their guidance at IMO.

Thank you to all my classmates, I'm grateful to be included in such a wonderful group. Special thanks go to my friends, from whom some are literally on the other side of the world. I wish to thank my parents for their support and encouragement throughout my study, without them I wouldn't have succeeded. Finally, my eternal gratitude to my boyfriend Jeroen, without his support, enthusiasm and faith, the past four years wouldn't have been so amazing.

Table of Contents

List of abbreviations

AIBN	2,2’-azobis(2-methylpropionitrile)
ATR-IR	attenuated total reflectance infrared
ATRP	Atom transfer radical polymerization
BiDoPAT	Bifunctional 2-([(Dodecylsulfanyl)carbonothioyl]sulfanyl)
n-BuA	*n*-Butyl acrylate
CTA	Chain transfer agent
DCC	N,N’-Dicyclohexylcarbodiimide
DMAP	4-(dimethylamino)pyridine
DMPA	Dimethoxy-2-phenylacetophenone
DoPAT	2-([(Dodecylsulfanyl)carbonothioyl]sulfanyl)
ESI-MS	Electrospray ionization mass spectrometry
GPC	Gel permeation chromatography
HDDA	Hexanediol diacrylate
^{1}H NMR	Proton nuclear magnetic resonance
2-HEA	2-Hydroxyethyl acrylate
MIP	Molecularly imprinted polymer
NaOH	Sodium hydroxide
NIP	Non-imprinted polymers
NMP	Nitroxide-mediated polymerization
Poly(*n*-BuA)	*n*-Butyl acrylate polymer
Poly(2-HEA)	2-Hydroxyethyl acrylate polymer
PS	Polystyrene
PVC	Polyvinylchloride
RAFT	Reversible-addition fragmentation transfer
TBP	Tributylphosphine
THF	Tetrahydrofuran

Abstract

Synthetic receptors, especially molecularly imprinted polymers (MIPs), are advantageous for bio(mimetic) sensors because of their stability, low production costs, long shelf life and easy synthesis. MIPs are polymer matrix particles containing imprints with a high affinity for their template molecule and after immobilization on a substrate they can be used as artificial receptors in biosensors. In order to produce cheap functionalized substrates, van Grinsven *et al.* fixated MIPs by stamping them in a polyvinyl chloride (PVC) adhesion layer. However, the use of PVC comes with several reproducibility problems caused by the detachment of MIP particles or adhesion of air bubbles during measurements in flow. The reproducibility of the biosensor can be improved by replacing the PVC with carefully designed polymer resins that are able to form a crosslinked network and form covalent bonds with the vinyl groups of the MIPs. The proposed resin comprises bifunctional polymers, which serve as macro crosslinkers by its vinyl groups at both ends, and a photo-initiator. The crosslinker properties make the resin photo-curable and allows for covalent attachment with the MIPs, as these particles are equipped with vinyl groups as well.

The bifunctional polymer was created in two main steps. First, reversible addition fragmentation transfer (RAFT) polymerization was performed in flow using a bifunctional RAFT-agent. RAFT provides polymers with high end group fidelity and control over the molecular weight. By choosing a more hydrophilic monomer (e.g. 2-hydroxyethyl acrylate (2-HEA)) the attachment of air bubbles during the flow measurements can be overcome. 2-HEA was polymerized with a molecular weight of 2000 $g \cdot mol^{-1}$. Next, a modification of the end groups via aminolysis and subsequent Michael addition yielded the (homotelechelic) vinyl functionalities, giving it the capability to crosslink. Even though UV-Vis indicated that there was 30% unreacted RAFT agent present, around 90% of the polymer was crosslinked without additional crosslinker, 1 mol% photo-initiator and exposure to 1 min to UV light. The thickness of the adhesion layer could be controlled with the concentration of the poly(2-HEA) and the rotation speed of the spincoater. Although it was difficult to quantify, optical microscopy pictures showed that the functionalized substrate had a minimal decrease of particles after exposure to a demi-water flow.

Nederlandse samenvatting

Synthetische receptors, met nadruk op *Molecularly Imprinted Polymers* (MIPs), zijn voordelig voor bio(mimetische) sensoren vanwege hun stabiliteit, lage productiekost, lange houdbaarheid en makkelijke synthese. MIPs zijn polymeer partikels met afdrukken in zijn matrix die een hoge affiniteit hebben voor hun doelwit molecule en na immobilizatie op een substraat kunnen ze gebruikt worden als artificiële receptoren in biosensoren. Om goedkope gefunctionaliseerde substraten te maken, van Grinsven *et al.* fixeerde de MIPs door ze op een polyvinylchloride (pvc) adhesie laag in te drukken. Het gebruik van pvc veroorzaakte echter reproduceerbaarheidsproblemen door het loskomen van MIP-partikels of de adhesie van luchtbellen wanneer men metingen in flow deed. De reproduceerbaarheid kan verbeterd worden door de pvc te vervangen door specifiek ontworpen polymeerhars of *resin* die een gecrosslinked netwerk kunnen vormen en covalente bindingen kunnen vormen met de vinyl groupen van de MIPs. Het voorgestelde *resin* mengsel bevat bifunctionele polymeren met acrylaatfunctionaliteiten aan de uiteindes, wat het in principe een macro crosslinker maakt. Samen met een foto-initiator wordt het *resin* hard wanneer het wordt geactiveerd door licht. Sinds de MIP-partikels ook vinylgroepen hebben, ontstaat er tijdens het uitharden een covalente binding van de resin met de MIP-deeltjes.

Het bifunctionele polymeer werd gemaakt in twee stappen. Ten eerste werd *reversible addition fragmentation transfer* (RAFT) polymerisatie uitgevoerd in flow met een bifunctioneel RAFT-agent. RAFT-polymerisatie heeft controle heeft over het moleculairgewicht en het behoud van de eindgroepen. Door een hydrofiel monomeer te gebruiken (b.v. 2-Hydroxyethyl acrylate (2-HEA)) kan het aanhechten van de luchtbubbels vermeden worden gedurende flow metingen. 2-HEA werd gepolymeriseerd met een moleculairgewicht van 2000 $g \cdot mol^{-1}$. Vervolgens werden de eindgroepen gemodificeerd via een aminolyse en vervolgens een *Michael addition* wat tot (homotelechelische) vinylfunctionaliteiten leidde en dus een crosslink eigenschap introduceerde aan het polymeer. Hoewel UV-Vis resultaten aanduiden dat er 30% niet gereageerde RAFT groepen aanwezig waren, ongeveer 90% van het polymeer was uitgehard zonder extra crosslinker, 1 mol% fotoinitiator en blootstelling aan licht voor 1 min. De dikte van de adhesie laag kon worden gecontroleerd door de concentratie van het poly(2-HEA) en de rotatiesnelheid van de spincoater. Hoewel het moeilijk was om te kwantificeren, optische microscopie afbeeldingen toonden aan dat het gefunctionaliseerde substraat een minimale daling in aantal partikels had na blootstelling aan een demi-water flow.

1 Introduction

Polymers are macromolecules that contain both natural variants, such as polysaccharides, polypeptides or polynucleotides, and synthetic variants, like plastics or resins. A polymer is a structure composed of many repeating units, such as amino acids in proteins, glucose units in polysaccharides, ethylene chloride in polyvinylchloride (PVC), and many other examples[1]. Both natural and synthetic polymers can be used in a variety of applications, ranging from medicine to material design. Natural polymers often have an intrinsic biocompatibility, which is advantageous when working closely with living cells, tissues or organisms. Nature can create complex materials with a limited amount of building block such as the four nucleotides to create DNA and 22 amino acids to make proteins[2]. There is a much broader range of building blocks available for synthetic polymers, which gives the opportunity to tune the chemical, mechanical and structural properties of the final polymers. One important application of polymers is their use as bioreceptor in biosensors.

In general, the components of a bio(mimetic) sensor can be classified into three parts: the bioreceptor, the transducer and the electronic readout[3]. The receptor is the heart of the sensor and recognizes the desired target from the sample. Using natural occurring receptors, such as enzymes, DNA, aptamers, antibodies or whole cells, is a great way to ensure a specific and selective binding of target molecules [4]. However, natural receptors work only in very specific physiological conditions and parameters such as pH or temperature. Another disadvantage is that the production costs of natural receptors can be very high, especially at larger scale. Synthetic receptors are an alternative route to consider when designing a sensor. There are several techniques that already exist such as dendrimers, organic and inorganic molecules, synthetic oligomers, nanoparticles and molecularly imprinted polymers (MIPs)[5]. MIPs have been especially interesting because of their stability, low production costs, long shelf life and easy synthesis. As demonstrated by van Grinsven *et al*., MIPs can be used as a bio-receptor and implemented in a biosensor[6]. Molecular imprinting has the same principle as a lock and key mechanism. The lock, in this case the MIP-particles is created around the target molecule that serves as the key. Functional monomers together with cross-linking agents form a matrix in which the template molecule is embedded (Figure 1, Polymerization). When removing the template, a specific binding site remains that matches the target molecule (Figure 1, Target removal). Not only does the size and shape determine the selectivity, the interaction with functional groups of the target molecule with the corresponding functional groups in the MIP leads to a high selectivity (Figure 1, Interactions). The MIP particles by itself are not enough to create a biosensor since there needs to be a translation from target binding to electronic readout.

First, the MIP and NIP particles need to be immobilized which can be done via several routes. Betlem *et al.* developed MIP screen printed electrodes were MIPs were mixed with carbon graphite ink to create printable sensors[7]. Kamra *et al.* covalently immobilised via a carbodiimide coupling for chemical sensing[8]. Among others, Thoelen *et al.* successfully immobilized MIP and NIP particles via a poly(p-phenylene vinylene) (PPV) derivate, OC1C10-PPV, or with cheaper polyvinylchloride (PVC) and used in sensor device based on impedance or the heat transfer method (HTM)[6, 9]. The HTM method, which was used by van Grinsven *et al*.[10] and later optimized by Geerets *et al*.[11], stated that this method enables fast and low cost measurements.

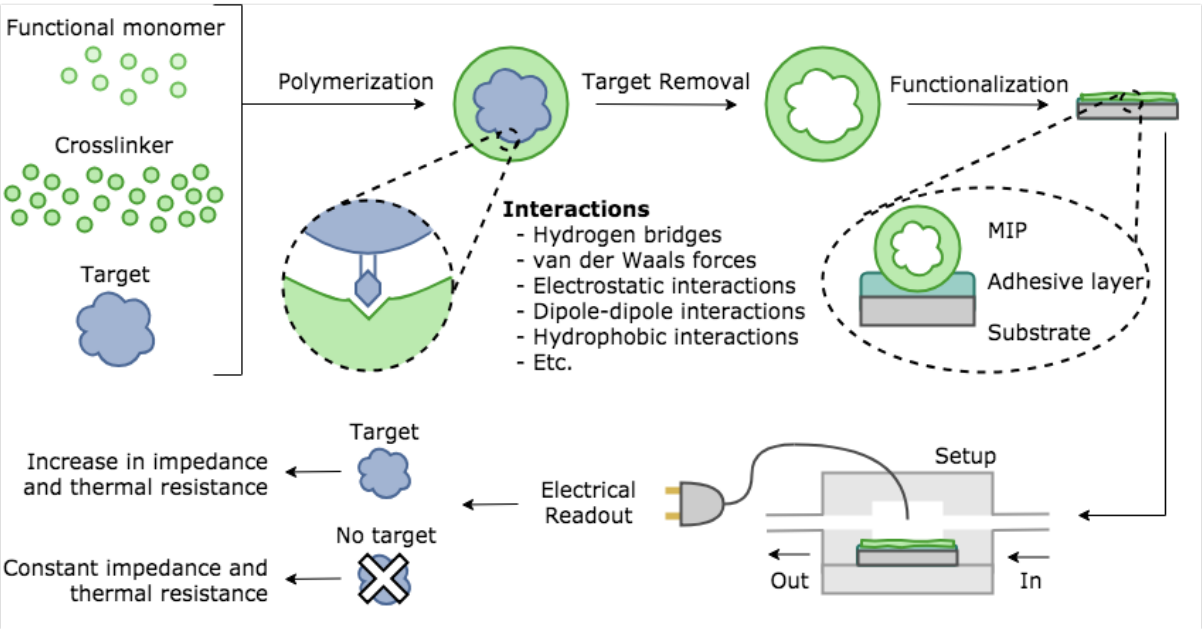

Figure 1: Schematic overview of the synthesis of molecularly imprinted polymers (MIPs) and how to implement them in a biosensor setup. Functional monomer and crosslinker (green) are polymerized around a target molecule (blue) leading to imprints with specific size, shape and interactions. After target removal, the MIPs are attached to a substrate via an adhesive layer. The functionalized substrate can be used in a setup which detects the presence of a target molecule in solution via impedance or thermal resistance.

Using a flowcell in combination with the HTM method and the impedance readout, binding of target molecules can be detected. The functionalized substrate is placed in a flow cell where solutions with different target concentrations can flow through and target binding results in a change of the thermal resistance and the impendence of the functional layer[3, 6]. To confirm the specificity of the measurements, the data from the MIP surface is compared with data from a control surface functionalized with non-imprinted polymers (NIPs). Both MIP and NIP particles are synthesized in the same manner, with the exception that NIPs are created without the presence of target molecules. Implementation of MIP and NIP particles had been executed by functionalizing a sensor chip with MIPs or NIPs using a polyvinyl chloride (PVC) adhesive layer. However, during measurements, particles would come loose and interfere with the readout (Figure 2).

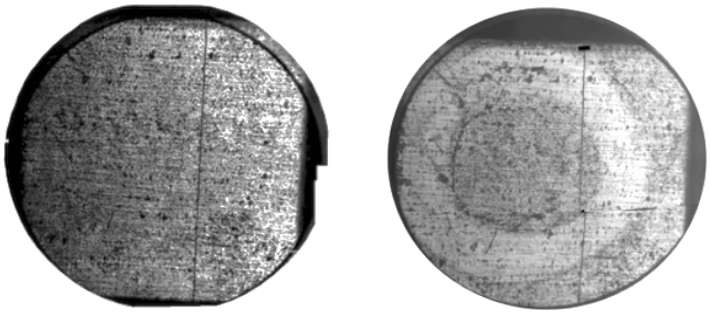

Figure 2: Microscopy pictures of a 1 cm by 1 cm functionalized aluminium substrate before (left) and after (right) use. The substrate is functionalized with Bisphenol A MIPs using polyvinylchloride (PVC) as adhesion layer. A clear reduction of the MIPs can be observed which is mainly due to mechanical friction.

Another problem was the accumulation of air bubbles in the flow compartment, which changes the R_{th} independently of binding of target molecules to the MIP particles. In conclusion, a more reproducible adhesive layer with better adhesion qualities than PVC but cheaper than OC1C10-PPV, is desired and a polymer resin is proposed as alternative.

The word resin is an umbrella term for a substance that with the right trigger, such as heat or UV-light, will crosslink and cure into a solid. For instance, polydimethylsiloxane (PDMS) is a silicon based organic polymer that can be used in soft lithography. When creating PDMS, a mixture of resin base and curing agent is thermally cured. The flexibility of the final product depends on the ratio between those two. A more specific example, as described by Tanodekew *et al.*, is the use of a photocurable resin in stereolithogrophy applications. The final gel had possible applications as implantation material[12]. Garcia *et al*. used a mixture of zinc oxide quantum dots (ZnO_{QDs}) and a resin to create an adhesive with antibacterial properties. With extra studies, ZnO_{QDs} can be a possible strategy to develop antibiofilm restorative polymers as improvement for dental remineralization over time[13]. Photosensitive resins can create two dimensional, and even three dimensional, structures with specific light exposure. Control over the structure creates the possibility to make polymer micro scaffolds that are modifiable, for example by the incorporation of growth factors.

The polymer resin designed for the MIP-based biosensor needs two main properties: the ability to crosslink and a hydrophilic character. Thus, a macro-crosslinker is specifically designed to meet both qualities. The resin itself consists of a mixture of photo-initiator and macro-crosslinker, making the adhesive layer curable by light. When the photo-initiator is activated, it will create radicals which will link the accessible vinyl groups in adjacent molecules. Moreover, the acrylate end-groups will also undergo an interaction with the free vinyl groups on the MIP particles itself, resulting in a strong covalent bond and therefore better adhesion (Figure 3).

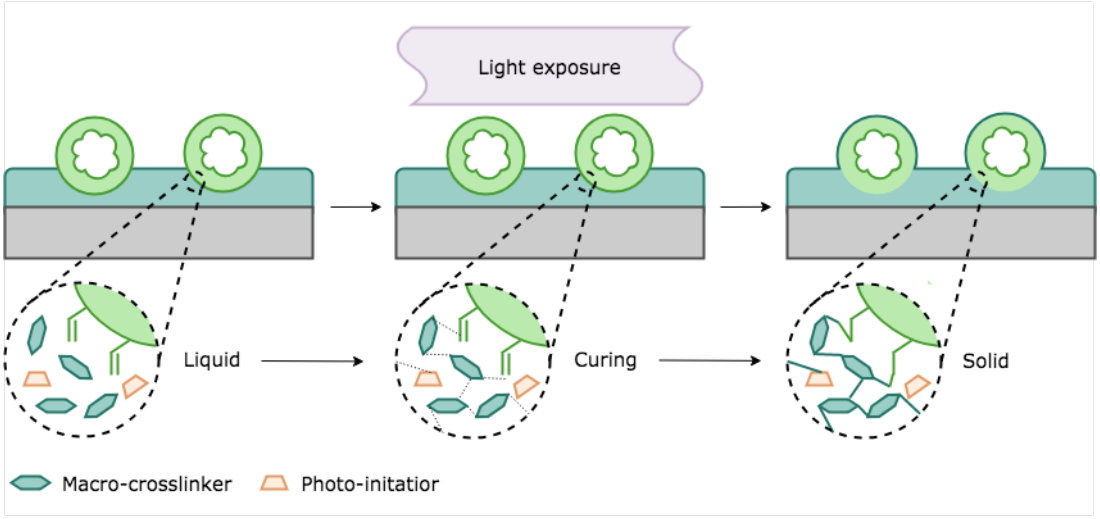

Figure 3: Representation of the curing mechanism of a resin designed for the attachment of molecularly imprinted polymer (MIP) particles (light green). The resin is a viscous liquid consisting of a macro-crosslinker (dark green) and photo-initiator (yellow). Light exposure activates the photo-initiator which will link unsaturated bonds during the curing step. Since the MIP particles also have unsaturated vinyl bonds, the resulting solid is a network that includes the MIPs.

Reversible-deactivation radical polymerization (RDRP), formally known as controlled radical polymerization (CRP), allows for the creation of tuneable macro-crosslinkers. With RDRP, one can create well-defined polymers with a precise molecular weight, low dispersity and specific composition. The three most important methods of RDRP are nitroxide-mediated polymerization (NMP)[14], atom transfer radical polymerization (ATRP)[15] and reversible addition-fragmentation transfer (RAFT) polymerization[16]. One of the advantages of RAFT is that it is compatible with a wide variety of monomers including styrenes, acrylates, methacrylates, vinyl esters, etcetera. Another advantage is that RAFT polymers can undergo a relatively easy post-modification of its end groups, for example the modification into thiols which subsequently can be used to undergo a thiol-ene click reaction[17]. In classical RAFT polymerization, there are three essential compounds: the initiator, the monomer and the chain transfer agent (CTA). The CTA, also known as RAFT agent, is typically formed by a dithioester together with a free radical leaving group (R) and a stabilizing group (Z). The effectiveness of the RAFT agent is determined by the R-group, the Z-group and the compatibility between the RAFT agent and the monomer. The mechanism of RAFT can be divided into five steps (Figure 4). In the first step, free radicals are created by the decomposition of an initiator which will react with a monomer, leading to propagating radicals (Figure 4, Initiation). Next, the propagating radical can transfer onto the thiocarbonylthio compound of the RAFT-agent which may result in the detachment of the R-group (Figure 4, Pre-equilibrium).

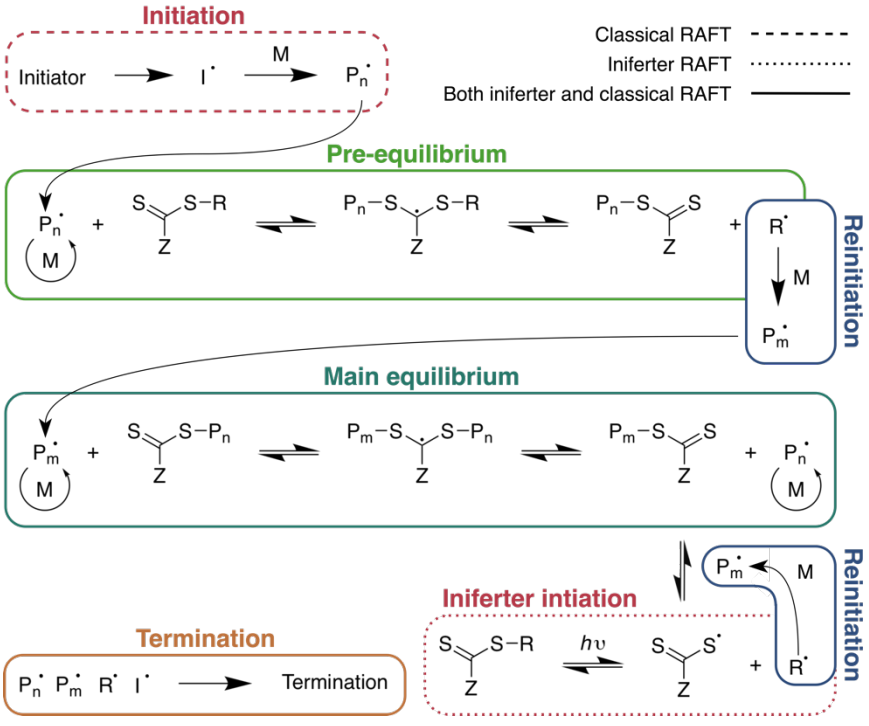

Figure 4: Overview of the reversible addition fragmentation transfer (RAFT) polymerization. Classical RAFT (dashed line) starts with the formation of propagating radicals via an initiator (red, dashed line). The propagating radical can transfer onto the RAFT agent forming the pre-equilibrium (light green). Via the reinitiation (blue), the R-group can generate new propagating radicals. Eventually, the main equilibrium is reached where there is a balance between dormant and active species (dark green). Eventually, radicals can react with each other to form non-reactive species (orange). In iniferter RAFT polymerization, there is no initiator but a splitting of the R-group from the RAFT agent under influence of light (red, dotted line). The cleaved off R-group will undergo reinitiation and the reaction will eventually have a similar pre-equilibrium, main equilibrium and termination as classical RAFT.

In the reinitiation step, new propagating radicals will be created by the formative radical of the R-group (Figure 4, Reinitiation). Since the release of the R-group leads to a new active center in the RAFT agent, the propagating radicals can again transfer onto the thiocarbonylthio compound resulting in a dormant intermediate with two chains (Figure 4, Main equilibrium). A rapid equilibrium, also referred as the main equilibrium, is formed between the dormant species and the active propagating radicals. The final step is the termination where two free radicals form a stable non-radical adduct (Figure 3, Termination). The chance that two propagating polymers will terminate is minimized since these are in their dormant state most of the time. Going a step further, the RAFT agents themselves can also function as an initiator resulting in a so-called photo-iniferter (INItiation transFER and TERmination) polymerization (Figure 4, Iniferter initiation). Instead of using an additional initiator to create radicals, light is used to cleave the R-group from the RAFT agent[18]. Avoiding the need of an initiator can be interesting for certain applications.

Using RAFT polymerization, new materials can be specifically designed for an application or problem in fields from material science to medicine. For example, Song *et al.* synthesized an amphiphilic, thermo-responsive graft copolymer using a novel macro-RAFT agent[19]. The copolymers self-assembled into spherical micelles which had temperature-induced release properties which, together with excellent biocompatibility and cellular uptake, opens the possibilities for controlled drug delivery[19]. For a similar purpose, Jiang *et al.* created block-copolymers with stimuli-responsive properties using a combination of RAFT and Pb(II)-initiated isocyanide polymerization[20]. Tochwin *et al.* also created thermoresponsive polymers but approached it differently by synthesizing a hyperbranched polymer via one-pot RAFT copolymerization of two different monomers, a crosslinker and the RAFT agent[21]. Zeng *et al.* made use of a self-catalyzed photo-initiated RAFT polymerization to create fluorescent polymeric nanoparticles. The particles are photo stable, show good biocompatibility and have aggregation-induced emission features which makes them ideal for biomedical applications[22].

Since the goal is to synthesize a macro-crosslinker, it is necessary to have at least two functional end groups instead of one. For this reason, a RAFT agent is made by coupling two RAFT-agents to each other via the R-group, resulting in a bifunctional RAFT agent (figure 5). After the initial polymer is made, the RAFT agent can be modified via aminolyis, resulting in a di-thiol chain by a spit via a nucleophile (Figure 5, Aminolysis)[23]. The thiocarbonylthio groups of the RAFT agent undergo a reaction with a nucleophile, to provide the thiol groups[23-24]. Primary and secondary amines are especially efficient to catalyse a thiol-ene reaction between thiols and acrylates[17]. With a base catalyst Michael addition, the protonated thiol functions as nucleophile and reacts with an electron-deficient carbon-carbon double bond to yield the coupled product (figure 5, Michael addition)[17, 25]. In this thesis, the bifunctional RAFT agent is based on 2-([(Dodecylsulfanyl)carbonothioyl]sulfanyl) (DoPAT) which is compatible with a variety of monomers, including styrene and acrylates[26]. If a diacrylate, such as hexanediol diacrylate, is used, the resulting polymer will have acrylic end groups (Figure 5, Green). The resulting macro-crosslinker will form covalent bonds with other acrylic functionalities including the vinyl groups present on the MIPs and NIPs, under influence of light. Thus, the MIPs themselves will be part of the polymer network (figure 3). The covalent interaction

of the resin with the MIP and NIP particles creates a recognition layer that is a whole unit instead of the receptors attached by non-covalent absorption.

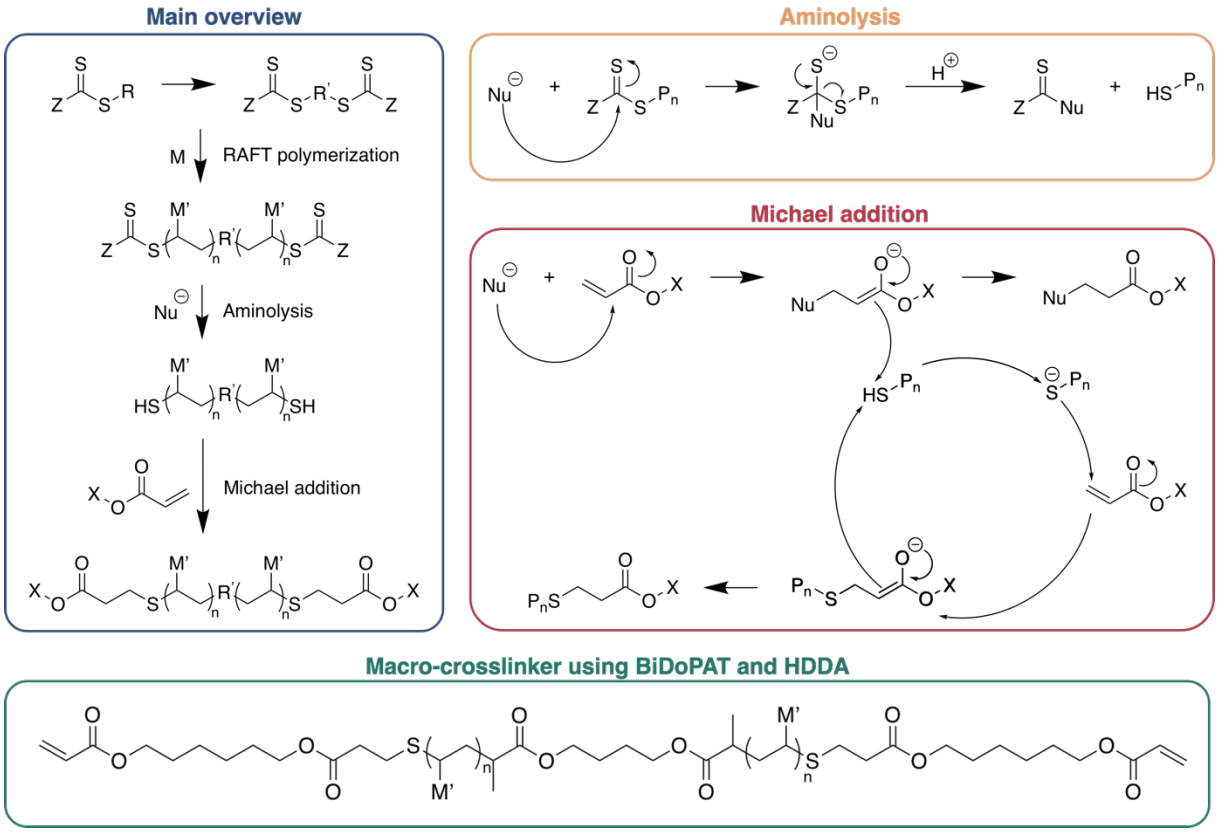

Figure 5: General overview to create the homotelechelic polymer. First, two RAFT agents are coupled via their R-group to generate a bifunctional RAFT-agent which is used to execute a RAFT polymerization (Blue). The end groups are modified with a nucleophile to thiols via aminolysis (Yellow). Via a Michael addition, an acrylate with a desired functionality (X) can be coupled via the thiol functionalities (Red). When using BiDoPAT as bifunctional RAFT agent and hexanediol diacrylate (HDDA) as end group functionality, a macro-crosslinker is generated (Green).

In conclusion, this thesis describes the development of a hydrophilic polymer resin which consists of a bifunctional crosslinker produced via RAFT polymerization and subsequent Michael addition. The ultimate goal is to improve the attachment of the MIP particles and avoid the adhesion of air bubbles, which both ameliorate the stability and reproducibility of the sensor output.

2 Materials and methods

2.1 Materials

The materials used for the following experiments were: 2,2'-azobis(2-methylpropionitrile) (AIBN, Sigma-Aldrich, 98%), 2-bromopropionic acid (Acros 99%), butyl acetate (Acros, 99%), *n*-butyl acrylate (*n*-BuA, Acros, 99%), carbon disulphide (Acros, 99.9%), N,N'-Dicyclohexylcarbodiimide (DCC, Acros, 99%), 4-(dimethylamino)pyridine (DMAP, Acros, 99%), dimethylformamide (VWR, pa.), dodecanethiol (Acros, 98%), hexanediol diacrylate (HDDA, Sigma-Aldrich, 80%), hexylamine (Acros, 99%), 2-hydroxyethyl acrylate (2-HEA, TCI, > 95%), sodium hydroxide (NaOH, VWR), styrene (S, Acros, 99.5%), tetrapropylammonium bromide (Acros, 98%) and tributylphosphine (TBP, Acros, 95%). All solvents used were obtained from commercial sources (Acros, VWR, Sigma-Aldrich) and used without further purification. All monomers (*n*-BuA, 2-HEA and S) were passed through a basic alumina column immediately before use to remove the inhibitor.

2.2 Characterization

Proton nuclear magnetic resonance (^{1}H-NMR) spectra were recorded in deutorated chorofrom ($CDCl_3$) on a Varian Inova 300 spectrometer at 300 MHz using a 5 mm probe.

Gel permeation chromatography (GPC) of the polymer samples were performed on a Tosoh EcoSEC HLC-8320GPC operated by PSS WinGPC software. The Tosoh EcoSEC was equipped with an autosampler, a PLgel 5.0 µm guard column (50 x 7.5 mm), followed by three PLgel 5 µm Mixed-C columns (300 x 8 mm) and a differential refractive index detector using THF as the eluent at 40 °C with a flow rate of 1 $mL \cdot min^{-1}$. The GPC system was calibrated using linear narrow polystyrene standards ranging from 474 to 7.5 x 106 $g \cdot mol^{-1}$ (PS (K= 14.1 x 10^{-5} $dL \cdot g^{-1}$ and α=0.70)), and toluene as a flow marker[27].

Electrospray ionization mass spectrometry (ESI-MS) was performed using a LTQ Orbitrap Velos Pro mass spectrometer (ThermoFischer Scientific) equipped with an atmospheric pressure ionization source operating in the nebulizer assisted electro spray mode. The instrument was calibrated in the m/z range 220-2000 using a standard solution containing caffeine, MRFA and Ultramark 1621. A constant spray voltage of 5 kV was used and nitrogen at a dimensionless auxiliary gas flow-rate of 5 and a dimensionless sheath gas flow-rate of 10 were applied. The S-lens RF level, the gate lens voltage, the front lens voltage and the capillary temperature were set to 50%, -90V, -8.5V, and 275 °C repectively. A 250 µL aliquot of a polymer solution was injected. A mixture of THF and methanol (THF-MeOH=3.2), all HPLC grade, was used as solvent[27].

Infrared spectra were recorded using an attenuated total reflectance infrared (ATR-IR) from BRUKER, Tensor-27. Between measurements, the crystal was cleaned with absolute ethanol. To measure the absorption spectra, a Cary 5000 UV-Vis-NIR spectrophotometer (Agilent) with a photometric performance in the 175-3300 nm range was used.

Polymer layers were applied using a Laurell WS-400BX-6NPP/Lite spin coater (Laurell Technologies). The thickness of the spincoated polymer layers were measured by a surface profilometer (Dektak®, Bruker). Optical microscopy images were made using an Axiovert40MAT inverted optical microscope (Zeiss, 5 Germany). A 5x magnification was used. With Image Composite Editor (ICE, Microsoft), various overlapping pictures were used to create one image per substrate.

2.3 Synthesis bifunctional polymer

2.3.1 Synthesis RAFT agent

Synthesis of the RAFT agent DoPAT[27]: a mixture of NaOH (1 eq.), dodecanethiol (1 eq.), acetone, water and tetrapropyl ammonium bromide was prepared and cooled to 0 °C with an ice bath. After a mixing period of 20 minutes, 2-bromopropionic acid was added and the reaction mixture was stirred overnight at room temperature. The solution was concentrated and then acidified with a HCl solution (2 M). The DoPAT precipitated as a yellow power which was collected and recrystallized from petroleumether (yield = 75%) (

Figure 6). ^{1}H NMR (400 MHz, Chloroform-*d*) δ (ppm) 10.2 (br, 1H), 4.85 (q, *J* = 7.4, 1H), 3.36 (t, *J* = 7.4 Hz, 2H), 1.70 (h, J = 7.4 Hz, 2H), 1.62 (d, *J* = 7.4, 0.7 Hz, 1H), 1.40 (br h, J = 7.4 Hz, 2H), 1.25 (br, 16H), 0.87 (t, *J* = 0.7 Hz, 3H).

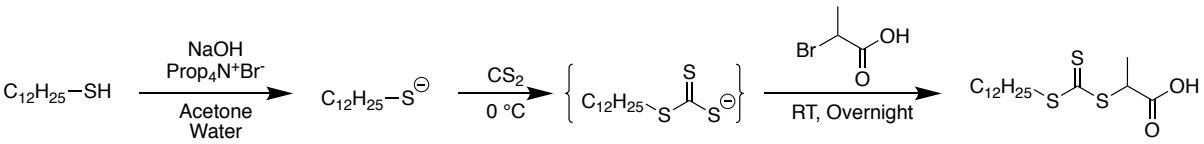

Figure 6: Reaction scheme of the synthesis of 2-([(Dodecylsulfanyl)carbonothioyl]sulfanyl) (DoPAT).

Synthesis of the bifunctional RAFT agent BiDoPAT[27]: an excess of DoPAT (3 eq.) and 1,4-butanediol (1 eq.) are dissolved in DCM over an ice bath. A mixture of DCC (2 eq.) and DMAP (0.1 eq.) in DCM is added dropwise to the first solution. The solution is stirred overnight at room temperature. An extraction with water and DCM was executed and the solvent was evaporated. The solid was purified with ethyl acetate over a column and recrystallized in petroleum ether (yield = 61%) (Figure 7). ^{1}H NMR (400 MHz, Chloroform-*d*) δ (ppm) 4.81 (q, *J* = 7.4 Hz, 2H), 4.25 – 4.02 (m, 4H), 3.35 (td, *J* = 7.3, 2.7 Hz, 4H), 1.76 – 1.64 (m, 8H), 1.58 (d, *J* = 7.4 Hz, 6H), 1.45 – 1.20 (m, 36H), 1.01 – 0.73 (m, 6H).

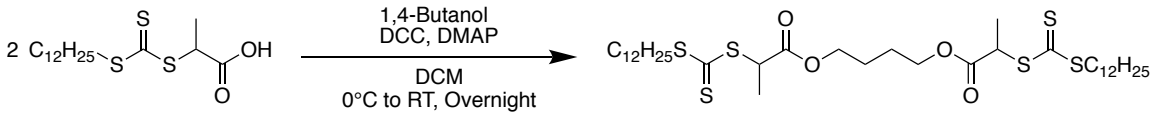

Figure 7: Reaction scheme of the synthesis of bifunctional DoPAT (BiDoPAT).

2.3.2 Batch RAFT polymerization of styrene with BiDoPAT

Polystyrene was synthesised by heating a degassed mixture of AIBN (0.1 eq.), BiDoPAT (1 eq.) and deinhibited styrene monomer (40 eq., 4.354 M) in butyl acetate (50 vol%) to 80 °C (Figure 8). The reaction mixture was put in an airtight flask and flushed with nitrogen gas for 5 minutes. Afterwards, the solution is kept under nitrogen atmosphere and placed in a pre-heated block of 80 °C. Quenching the polymerization was done by placing the flask in an ice bath. To purify the polymer, the BiDoPAT polystyrene (PS) was precipitated in cold methanol. The product was analysed with GPC and ^{1}H NMR.

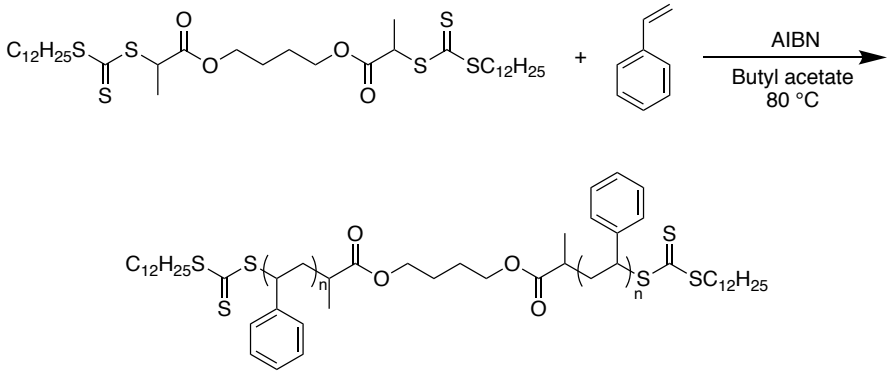

Figure 8: Reaction scheme of RAFT polymerization using BiDoPAT and styrene monomer.

2.3.3 Thermal initiated RAFT polymerization of n-BuA and 2-HEA with BiDoPAT

Thermoinitiated reactions were executed in a flow setup with perfluoroalkoxy (PFA) tubing wrapped around a holder in an oil bath of 100 °C. The reactor volume is 2 mL and the flow was generated by an Azura® HPLC pump from Knauer. The styrene monomer, the *n*-BuA monomer and the 2-HEA monomer were tested in this setup. Since the temperature is close to or over the boiling point of the used solvents, a backpressure of 100 psi was used. Azobisisobutyronitrile (AIBN) was added as initiator in all the reactions.

***n*-BuA:** BiDoPAT (1 eq.) and *n*-BuA monomer (30 eq., 2.778 M) were dissolved in 1,6-dioxane (60 vol%) and the solution was purged with nitrogen gas. The *n*-BuA polymer (poly(*n*-BuA)) with residence times of 1 min, 2 min, 5 min, 16 min and 30 min were analysed with ^{1}H NMR, GPC and ESI-MS.

2-HEA: BiDoPAT (1 eq.) and 2-HEA monomer (30 eq., 0.871 M) were dissolved in 1,6-dioxane (90 vol%) and the solution was purged with nitrogen. The residence times were of 1 min, 2 min, 5 min, 16 min and 30 min. To purify the 2-HEA polymer (poly(2-HEA)), it was precipitated in cold hexane. Analysis was done with ^{1}H NMR, GPC and ESI-MS.

Styrene: BiDoPAT (1 eq.) and styrene monomer (60eq., 4.5350 M) were dissolved in 1,6-dioxane (50 vol%) and the solution was purged with nitrogen. The residence times were of 5 min, 15 min and 30 min. To purify the polymer, it was precipitated in cold methanol. Analysis was done with ^{1}H NMR and GPC.

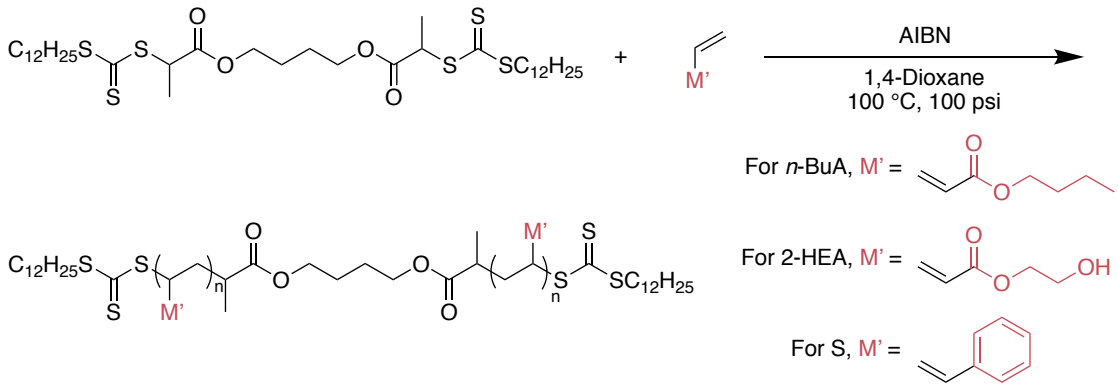

Figure 9: Reaction scheme of thermal induced RAFT polymerization using BiDoPAT and *n*-Butyl acrylate (*n*-BuA), 2-hydroxyethyl acrylate (2-HEA) or styrene (S) monomer. The variable M' for each monomer is indicated in red.

2.3.4 Photoinitiated RAFT polymerization of *n*-BuA and 2-HEA with BiDoPAT

Photoiniferter reactions were executed in a flow setup with Teflon tubing wrapped around a UV-lamp of 365 nm. The reactor volume is 1 mL and the flow is generated by an Azura® HPLC pump from Knauer.

***n*-BuA:** BiDoPAT (1 eq.) and *n*-BuA monomer (40 eq., 3.475 M) were dissolved in butyl acetate (50 vol%) and the solution was flushed with nitrogen gas for 5 minutes. Afterwards, the flowrate was adjusted to test the residence times of 2 min, 5 min, 10 min, 15 min, 20 min, 30 min and 120 min. Before and between sample collection, the reactor was left to stabilize for two times the residence time. The polymer was analysed with ^{1}H NMR, GPC and ESI-MS.

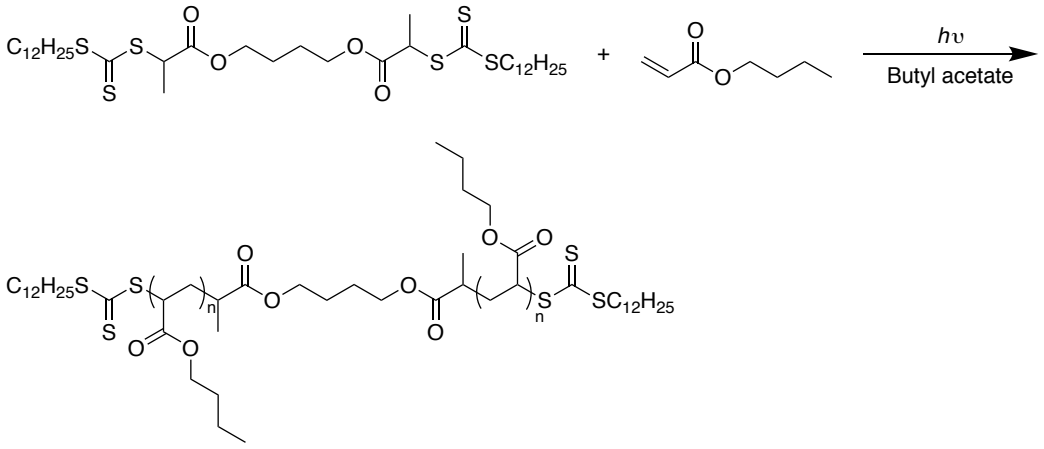

Figure 10: Reaction scheme of photoinitiated RAFT polymerization using BiDoPAT and *n*-Butyl acrylate (*n*-BuA) monomer.

2.3.5 Aminolysis and thiolene click reaction

Per equivalent bifunctional polymer, there are at least four equivalents of hexylamine used (Figure 11). For the Michael addition, the diacrylate HDDA was used.

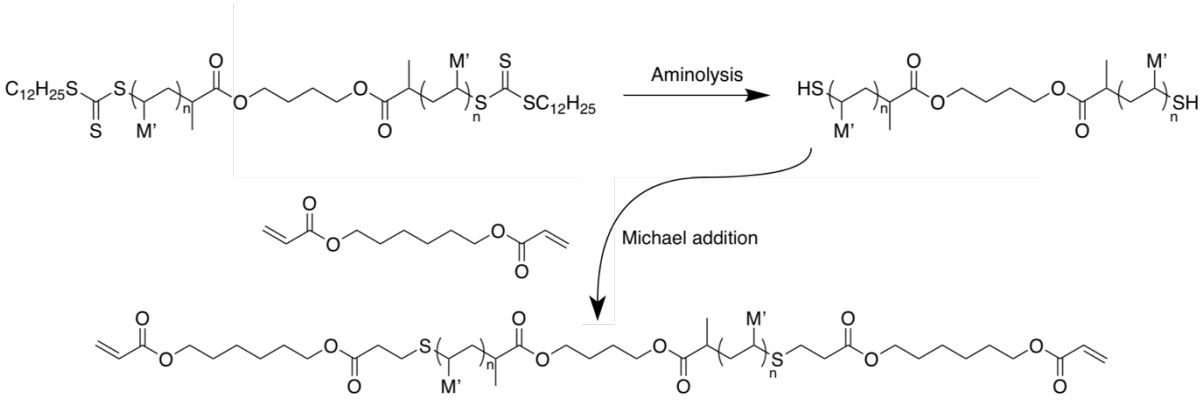

Figure 11: Scheme of the effect of the effect of aminolysis and the Michael addition on a polymer with homotelechelic end groups. The thiol-ene click reaction occurs between the thiol functionalities of the polymer and the vinyle group of the 1,6-hexanediol diacrylate.

Styrene: PS (1 eq., 0.151 M) of the batch reactions was dissolved in DMF (75 wt%). An excess of hexylamine (30 eq.) and a trace of TBP were added as catalyst and reducing agent to avoid disulphide formation respectively. The mixture was stirred for at least two hours at ambient temperature. After purification by precipitation in cold methanol, the polymer was collected and analysed by both ^{1}H NMR and GPC. For the thiol-ene click reaction, the polymer (1 eq., 0.160 M) is dissolved in THF and the reaction was started by adding an excess of HDDA (10 eq.) and a drop of TBP (0.1 eq.). After the click reaction, the polymer was again characterized by GPC.

The PS modification was also executed *in situ.* PS (1 eq., 0.119 M) of the batch reactions was dissolved in THF (75 wt%) together with excess of hexylamine (5 eq.) and an excess of HDDA (10 eq.). The mixture was stirred overnight at ambient temperature. After purification by precipitation in cold methanol, the polymer was collected and analysed by GPC.

2-HEA: there were two different protocols of the poly(2-HEA) modification. The first protocol used 2-HEA polymer (1 eq., 0.148 M) dissolved in THF (75 wt%) together with of hexylamine (5 eq.) and an excess of HDDA (10 eq.). After stirring at ambient temperature overnight, the polymer was precipitated in cold hexane. The second protocol was the same but with higher excess of hexylamine (30 eq.) and an excess of HDDA (5 eq.). Characterization was executed by both GPC and ESI-MS. UV-Vis samples from before and after the modification reaction were prepared with the same molar concentration in absolute ethanol.

2.4 Preparation of functionalized substrates

The light source that was used to cure the polymer resins was provided by an OmniCure® containing a 100 W lamp with a broad spectral output ranging from 250 nm to 450 nm. A Quartz Fiber Light Guide was used to guide the light to a fixed position. Samples were placed on a standard position, 15 cm under the opening of the light source. The energy of the light at the standard position was measured at different iris openings. Different light intensities, namely 5 mW·cm^{-2}, 10 mW·cm^{-2} and 15 mW·cm^{-2}, were tested with a mixture containing HDDA crosslinker and DMPA initiator. Different samples were prepared with a mixture with (5 mol%) or without DMPA and subsequently cured for 0 min, 5 min or 10 min. Two types of modified polymer were tested at 15 mW·cm^{-2}: modified PS and modified poly(2-HEA). The M_n of the PS and the poly(2-HEA) were respectively 1300 g·mol^{-1} and 2000 g·mol^{-1}. Several parameters were varied including the exposure time, the DMPA concentration and the amount of HDDA. The polymer and crosslinker mixture was diluted with THF (0.5 M) in which the desired amount of initiator was dissolved.

Since these crosslinked structures do not dissolve in THF, the percentage of resin that is left after thoroughly rinsing with THF can be determined (Equation 1). All samples were dried with a nitrogen flow before determination of the weight with an analytical balance

$$Resin\ present = \frac{W_{\text{After}} - W_{\text{Substrate}}}{W_{\text{Before}} - W_{\text{Substrate}}} \qquad \text{Equation 1}$$

Before use, the aluminium substrates were cleaned subsequently by isopropanol, acetone and MilliQ for five minutes in an ultrasonic bath. 50 µL of different resin mixtures were spincoated for one minute at different speeds. The maximal concentration was made by dissolving 1.28 g modified 2-HEA polymer of around 2000 g·mol^{-1} in 1 mL THF. The lower concentrations were made by diluting the maximal stock concentration to 0.32 g·mL^{-1} and 0.16 g·mL^{-1}. For each concentration, 5 mol% initiator was added with respect to the amount of polymer present. Each equivalent polymer corresponded thus with approximately 0.05 eq. DMPA. Three different speed settings were tested: 3000 rpm, 4000 rpm and 5000 rpm. After spincoating, the solvent was evaporated, a scratch was made in the polymer layer and the substrate was exposed to UV light for 1 min. The height difference between the substrates surface and the cured polymer layered was measured by a height profilometer.

Three types of particles were used: suspension polymerization NIPs, bulk nicotine NIPs and bulk nicotine MIPs. The MIP and the NIP particles, which were characterized by ATR-IR and microscopy, were added to the adhesive layer on the substrate and cured. First, the round suspension NIPs were tested for adhesion. An adhesion layer was spincoated using modified 2-HEA polymer of around 2000 g·mol^{-1}. The polymer was dissolved together with 5 mol% DMPA in THF and spincoated on top of a clean aluminium substrate. NIP particles were carefully distributed over the resin layer and the whole substrate was cured under UV for 1 min. The functionalized substrates were studied with an optical microscope to visualize detachment of particles.

3 Results and discussion

3.1 Synthesis of bifunctional polymers

3.1.1 Batch polymerization of styrene and further modification

Both the synthesis of BiDoPAT, several batch polymerizations and the thiol-ene click reaction was successfully executed by Vandenbergh *et al*. where a direct proportional growth of PS can be observed with increasing reaction times[27]. The synthesis of the PS and further modification reactions function as a proof of principle. Per equivalent bifunctional polymer, there are at least four equivalents hexylamine necessary to completely reduce the end groups of the polymer to thiols (Figure 11) When doing the aminolysis and the Michael addition *in situ,* a little excess of hexylamine is required. In theory, there are only two equivalents of 1,6-Hexanediol diacrylate (HDDA) necessary to obtain the desired polymer. However, an excess of HDDA was used to lower the risk to create multi-segmented polymers. During the aminolysis, the reduction of the RAFT-agent functionality to a thiol will result in the decrease of the M_n (Figure 11). Similarly, addition of the diacrylates in the Michael addition step increases the M_n (Figure 11). When the aminolysis and the Michael addition are performed separately, this shift in M_n is detectable with GPC (Figure 12). Since the weight of the Z-group together with the carbon and the sulphur is approximately the same as HDDA, the M_n of the start product and the final product is also similar. To calculate the M_n, the small distribution at lower molecular weights was not considered since it is most likely a trace of the hexylamine or HDDA.

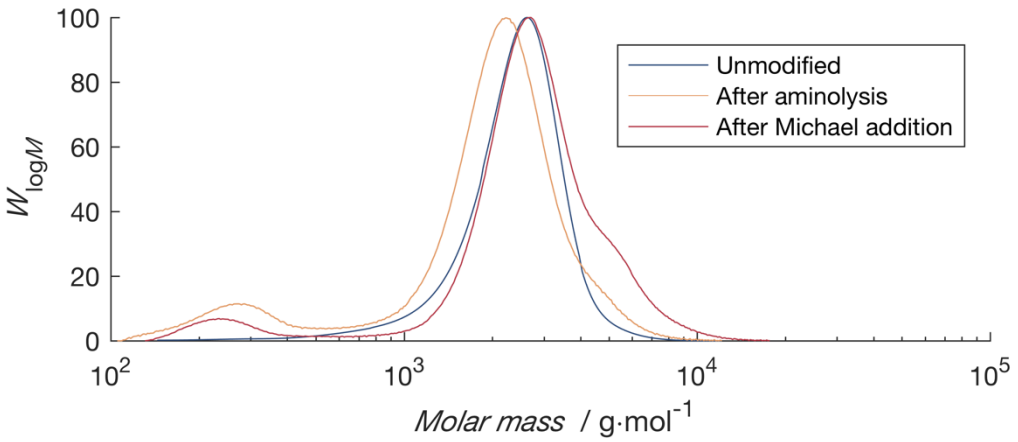

Figure 12: Molecular weight distribution of polystyrene before modification (blue), after aminolysis (yellow) and after the Michael addition (red).

After a reaction time of 6 hours, PS with a M_n of 2100 g·mol^{-1} and a $Đ$ of 1.17 was obtained. The molecular weight distribution meets the expectations, since the aminolysis reduces the M_n from 2100 g·mol^{-1} to 1900 g·mol^{-1}. The maximum peak of the M_n after the Michael addition is approximately the same as before the modification but the M_n is increased to 2700 g·mol^{-1}. The molecular weight distribution of the poly(2-HEA) (Figure 12, Red) has a slight shoulder to a higher molecular weight, possibly due to coupling of two polymer chains to the same diacrylate molecule. The manifestation of the shoulder lies approximately around 5000 g·mol^{-1}, which is circa twice the

value of the M_p (2600 g·mol^{-1}) and thus suggests that there is indeed coupling between two PS molecules. The thiol-ene click reaction was also performed *in situ* (Figure 13).

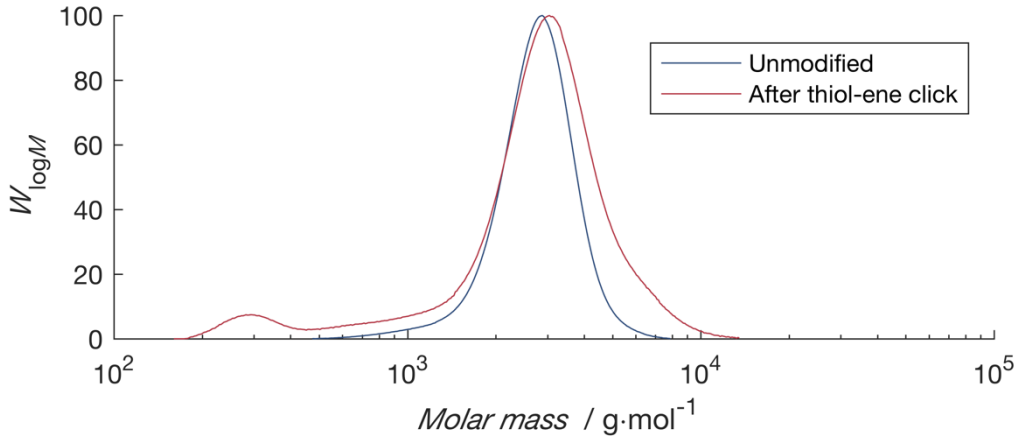

Figure 13: Molecular weight distribution of polystyrene before modification (blue) and after the thiol-ene click reaction (red).

The M_n of both the unmodified and the modified PS is 2500 g·mol^{-1}. The peak of the modified PS (Figure 13, Red) does not show a shift to lower molecular masses. Moreover, during the reaction there was a visible shift in colour from bright yellow to transparent. The reduction of the yellow colour is due to the breaking of the thiocarbonylthio bonds from the RAFT-agent, which might be an indication of a successful aminolysis.

3.1.2 Thermal initiated polymerization of styrene in flow

Under the right conditions, continuous flow reactions provide materials with lower dispersity and higher end group fidelity. Moreover, while batch reactions are usually carried out on milligram scale, continuous flow allows for the upscaling making it advantageous for industry. The main disadvantage of batch polymerization comes from the intensity gradients, whether it be heat or light, leading to a loss of reaction efficiency. In contrast, the reactors for continuous flow reactions are designed to have an optimal surface to volume ratio[28]. Since styrene is typically more difficult to polymerize through photoinitiation, photoiniferter reactions in flow were not tested. Instead, thermal initiated reactions using AIBN were performed. Styrene is a slow propagating molecule and for this reason a higher monomer to RAFT-agent ratio was used when compared to the batch polymerization (1:60 to 1:40). Thus, to compensate for the slower propagation, and by that the lower conversion, more monomer was used. Residence times of 5 min, 15 min and 30 min were tested, which is significantly faster when compared to the 6 h of batch polymerization. Since the half-life time of AIBN is 8 min, higher residence times were not tested because after a while all the initiator would have been consumed[29]. An overlay of the molecular weight distribution was plotted (Figure 14).

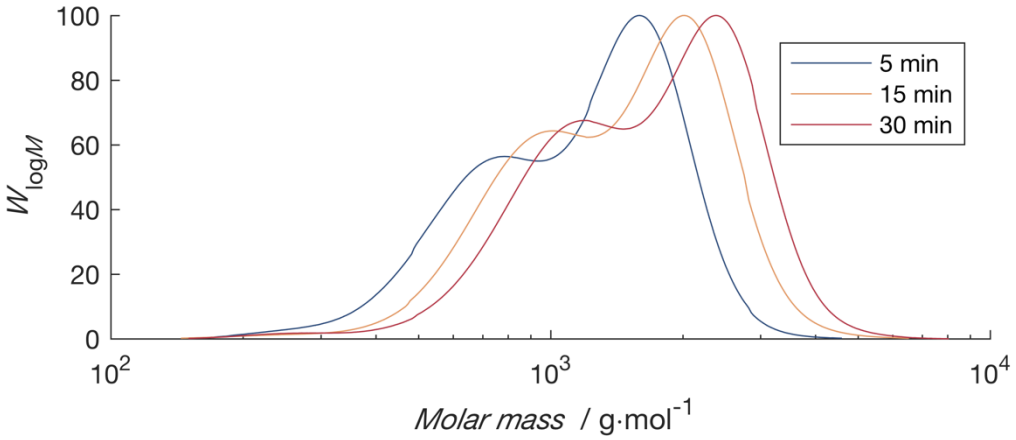

Figure 14: Overlay of molecular weight distributions of polystyrene in thermal initiated flow for different residence times going from 5 min to 30 min. Polymerization was executed with 1 eq. BiDoPAT and 60 eq. S in 1,4-dioxane in presence of 0.1 eq. AIBN at 100 °C.

The GPC output shows clearly two distributions, with the smaller distribution manifesting at a M_n approximately half the M_n of the larger distribution. Possible explanations, however unlikely, could be that only one side of the BiDoPAT RAFT agent is active or that the RAFT agent spilt into two. For this reason, only the batch PS was used for further modifications. As mentioned by Beaten *et al.*, there is further optimization needed when using slower propagating monomers such as styrene[29]. Further flow polymerizations will be executed with *n*-BuA and 2-HEA monomer.

3.1.3 Thermal initiated polymerization of *n*-BuA

Baeten *et al.* optimized a thermal initiated polymerization reaction in flow for DoPAT with several acrylate monomers[29]. Here, similar experiments were executed but with BiDoPAT instead of DoPAT. To visualize the increase in M_n over time, the overlay of the GPC outputs for different times was plotted (Figure 15).

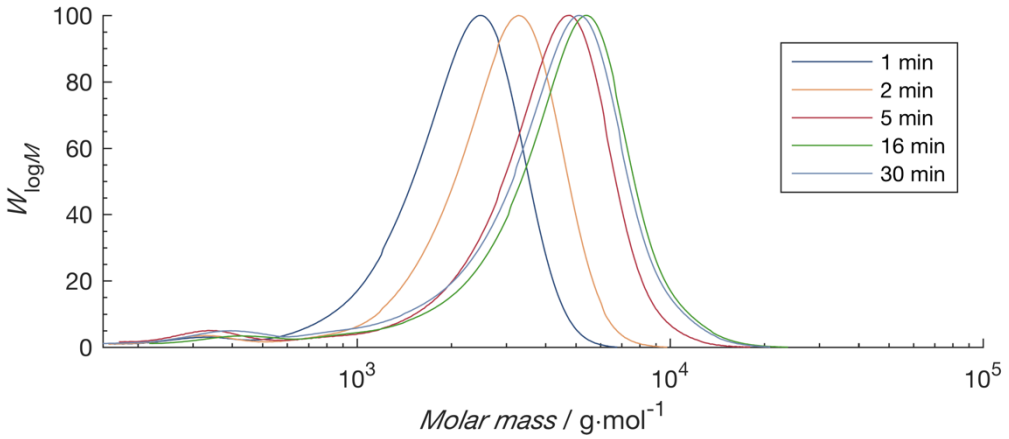

Figure 15: Overlay of molecular weight distributions of different n-BuA polymers with varying residence times going from 1 min to 30 min. Polymerization was executed with 1 eq. BiDoPAT and 30 eq. n-BuA in 1,4-dioxane in presence of 0.1 eq. AIBN at 100 °C.

Until a residence time of 16 min, these is a direct proportional growth of the *n*-BuA polymer with increasing residence times. With increasing residence times, the M_n increased from 1900 g·mol^{-1} (1 min) to 3900 g·mol^{-1} (16 min), before it decreased back to 3500 g·mol^{-1}. Baeten *et al*. concluded that the optimized reaction time for their polymers was 16 min which is twice the half-life time of AIBN at 100 °C[29]. The effect of the decreasing initiator concentration at higher residence times might explain the outlier of 30 min.

The M_n and the dispersity, which were determined by GPC, were plotted against the conversion, which was determined by ^{1}H-NMR (Figure 16). When calculating the M_n, the small distribution at low molecular weights was not taken into account since it would have let to an underestimation of the overall M_n (Appendix, Table 1).

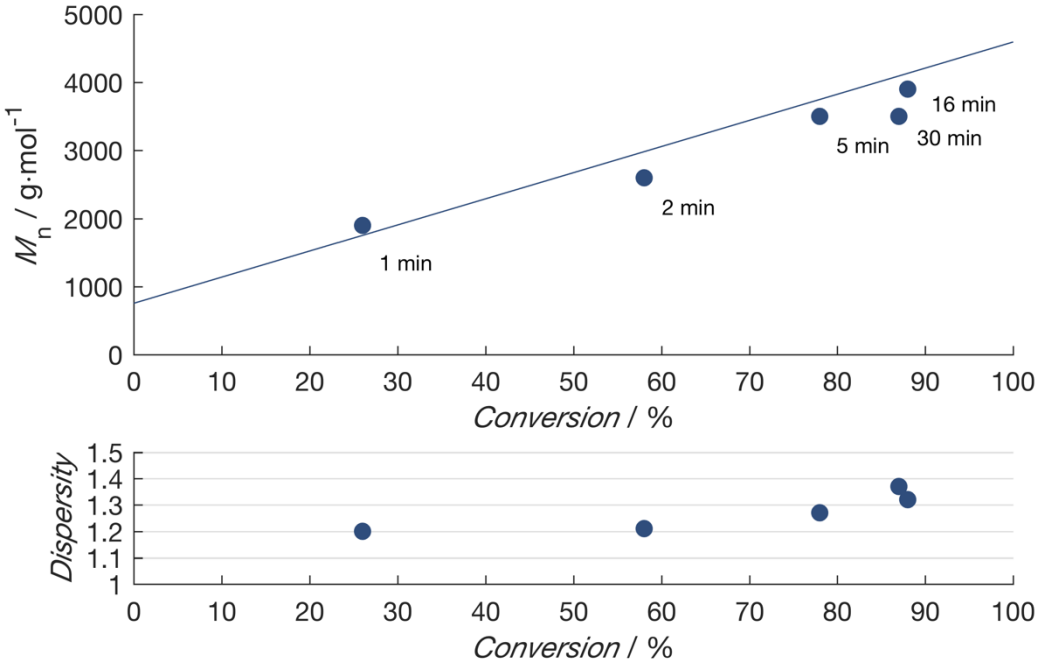

Figure 16: M_n (upper graph) and dispersity (lower graph) determined by GPC plotted against the conversion of different *n*-BuA polymers with varying residence times going from 1 min to 30 min. Polymerization was executed with 0.1 eq AIBN, 1 eq. BiDoPAT and 30 eq. *n*-BuA in 1,4-dioxane at 100°C. For the molecular weight distribution, a theoretical line was determined and plotted with the GPC output.

With exception of the data point from 30 min, the theoretical linear correlation between the M_n and the conversion (Figure 16, upper graph, line) corresponds well with the measured GPC values. One can conclude that at lower or equal to 16 min the growth of the polymer grows is directly proportional. The dispersity of the polymers stays within an acceptable range for a controlled polymerization reaction varying from 1.19 to 1.36 (Appendix, Table 1).

From the conversion, the $\ln([M]_0/[M]_t)$ term can be calculated (Equation 2). The relationship between the $\ln([M]_0/[M]_t)$ and the reaction time first increases with time and then stagnates after approximately 16 min (Appendix, Figure 34). Thus, there is no inhibition period and a maximum conversion of 78% was reached.

$$\ln\left(\frac{[M]_0}{[M]_t}\right) = \ln\left(\frac{1}{1-conversion}\right) \qquad \text{Equation 2}$$

The preservation of the end groups is important since they are necessary in the further modification of the polymer. The end group fidelity was confirmed with ESI-MS, indicating homotelechelic RAFT polymers (Figure 17).

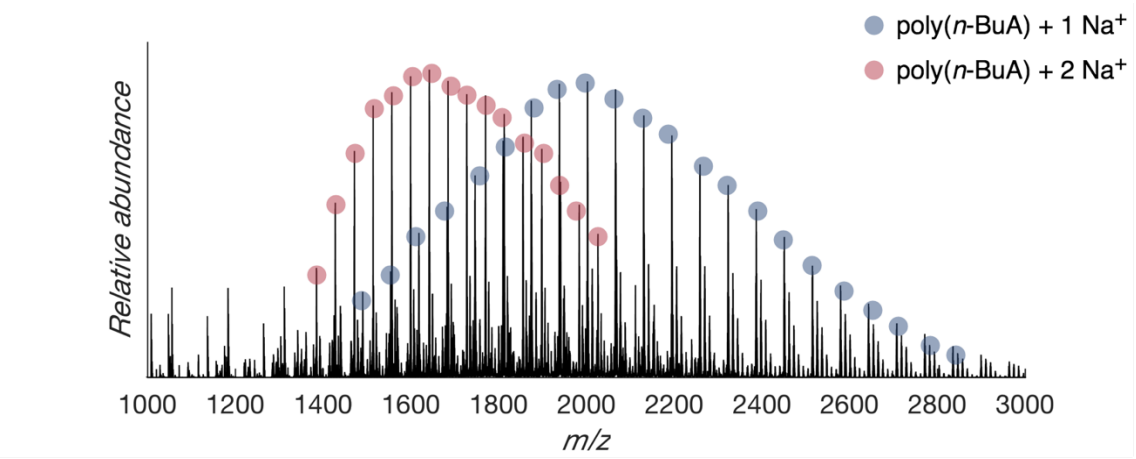

Figure 17: ESI-MS for single charged poly(*n*-BuA) (blue) and double charged poly(*n*-BuA) (red). Polymerization was executed with 1 eq. BiDoPAT and 30 eq. n-BuA in 1,4-dioxane in presence of 0.1 eq. AIBN at 100 °C for a residence time of 16 min.

The distribution on the left (Figure 17, Red) is double charged poly(*n*-BuA) while the one on the right (Figure 17, Blue) is single charged poly(*n*-BuA). The RAFT end groups are present, making the poly(*n*-BuA) polymer suitable for further modification. Because *n*-BuA polymers are difficult to precipitate, the residual solvent and monomer were evaporated after polymerization, meaning that there could still be traces of AIBN left in the poly(*n*-BuA) mixture. To lower the risk of side reactions in the curing of resin later, iniferter polymerization with *n*-BuA was investigated.

3.2.4 Photoiniferter polymerization of *n*-BuA

Different residence times going from 2 min to 120 min were investigated. Again, to visualize the increase in M_n over time, the overlay of the GPC outputs for different times was plotted (Figure 18).

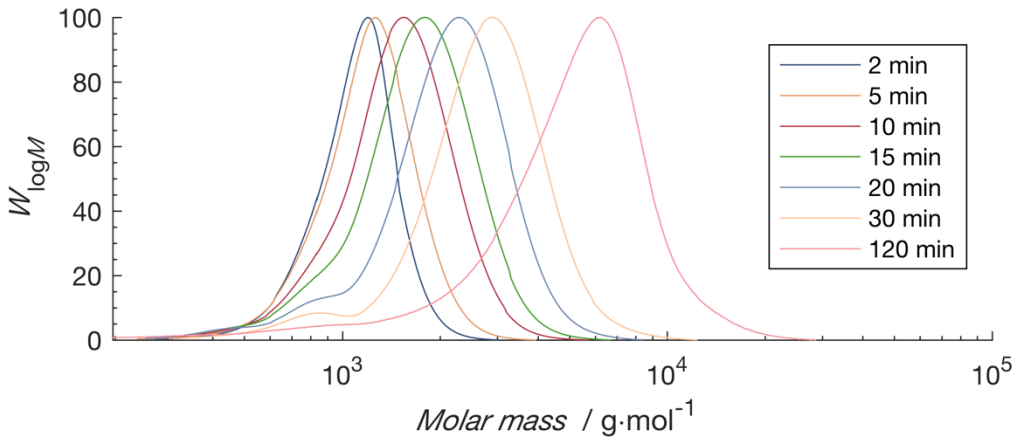

Figure 18: Overlay of molecular weight distributions of different *n*-BuA polymers with varying residence times going from 2 min to 120 min. Polymerization was executed with 1 eq. BiDoPAT and 40 eq. *n*-BuA in butyl acetate under UV light.x

As expected, the M_n increases with an increasing residence time (Figure 18). The little shoulder observed at the smaller end of the mass distribution (Figure 18, 20 min and 30 min) was excluded for the number average molecular weight calculation (Figure 19). The M_n increases with a direct proportional growth of the *n*-BuA polymer from 1000 g·mol^{-1} to 4700 g·mol^{-1} (Appendix, Table 2). Wenn *et al.* investigated different initiators under UV-light, including iniferter polymerization with DoPAT[18a]. Thus, the coupling of DoPAT to form BiDoPAT does not influence its ability for successful iniferter polymerizations.

The molecular weight and the dispersity were determined by GPC and plotted against the corresponding conversion (Figure 19,). The $\ln([M]_0/[M]_t)$ versus the reaction time was again plotted (Figure 35).

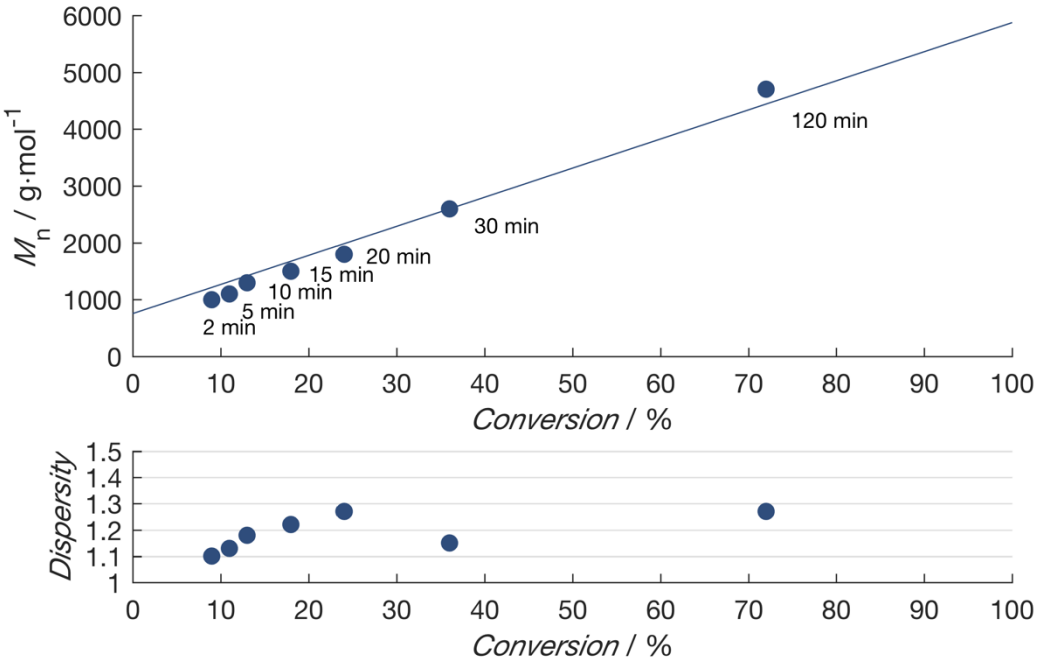

Figure 19: M_n (upper graph) and dispersity (lower graph) determined by GPC plotted against the conversion of different *n*-BuA polymers with varying residence times going from 2 min to 120 min. Polymerization was executed with 1 eq. BiDoPAT and 40 eq. *n*-BuA in butyl acetate under UV light. For the molecular weight distribution, a theoretical line was determined and plotted with the GPC output.

The theoretical linear correlation between the M_n and the conversion (Figure 19, upper graph, line) corresponds well with the measured GPC values. Since the polymer grows directly proportional with the residence time, it gives an indication that the reaction is indeed controlled. The dispersity of the polymers stays within an acceptable range for a controlled polymerization reaction varying from 1.10 to 1.27 (Appendix, Table 2). When comparing the conversion of iniferter polymerization and classical thermal RAFT, there is respectively a maximum conversion of 72% in 120 min and 88% conversion in 16 min. Thus, iniferter polymerization is much slower, confirming the conclusions of Wenn *et al*.[18a].

The $\ln([M]_0/[M]_t)$ versus reaction time plot is linear, indicating a constant radical concentration. Compared with the $\ln([M]_0/[M]_t)$ versus time plot of the thermal RAFT polymerization (Figure 34),

the linearity is more pronounced in the corresponding plot of the photoinitiator reaction (Figure 23). The photoiniferter reaction keeps a constant radical concentration for a longer time but does not reach the high conversions as when AIBN is used.

Again, the preservation of the end groups was confirmed with ESI-MS since they are necessary in the further modification of the polymer (Figure 20).

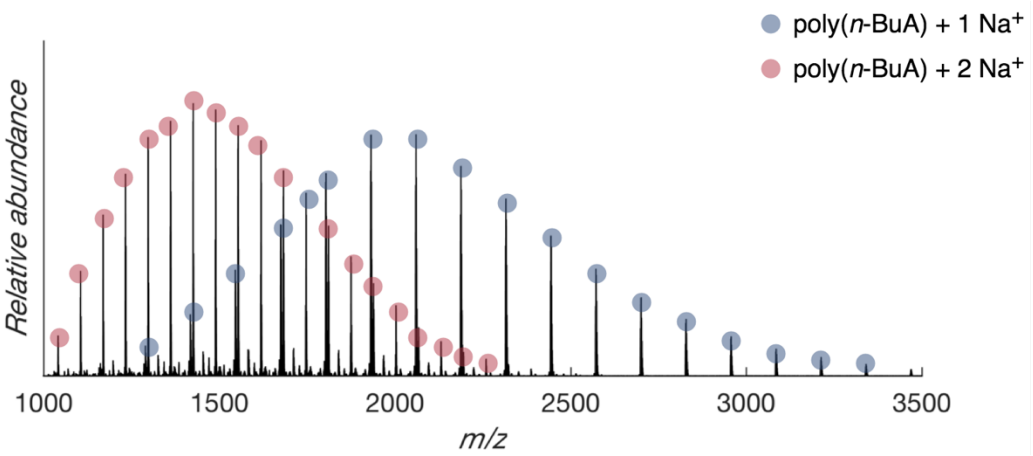

Figure 20: ESI-MS for single charged poly(*n*-BuA) (red) and double charged poly(*n*-BuA) (blue). *n*-BuA was polymerized with 1 eq. BiDoPAT for different residence times. Polymerization was executed with 1 eq. BiDoPAT and 40 eq. *n*-BuA in butyl acetate under UV light.

The distribution on the left is double charged poly(*n*-BuA) while the one on the right is single charged poly(*n*-BuA). In conclusion, the poly(*n*-BuA) is suitable for a thiol-ene click reaction but was not further investigated due to limited time. Because of its hydrophilic properties, poly(2-HEA) got priority to create the polymer resin.

3.1.5 Thermal initiated polymerization of 2-HEA

Since it was more favourable that the polymer resin had hydrophilic properties, the hydrophilic monomer 2-HEA was investigated. Compared to *n*-BuA, due to solubility, a lower monomer concentration was chosen, while keeping the type of solvent constant. Unfortunately, reliable molecular weight distributions could not be determined since the behaviour of the hydrodynamic volume of the hydrophilic poly(2-HEA) on a THF-GPC is difficult to predict and suitable Mark-Houwink parameters were not available. Vargün *et al.* noted that poly(2-HEA) was insoluble in most common solvents due to high molecular weights and strong intermolecular hydrogen bonding[30]. Because of the poly(2-HEA) hydrophilicity, it has a better solubility in water and thus GPC measurements with water as eluents are most likely more suitable for these polymers. For this reason, the normalized intensity was plotted against the elution volume (Figure 21). In the overlay of the elution volumes, the peak of the polymers was plotted as a full line, while the peaks at higher elution volumes, and thus lower molecular weights, was indicated as a dotted line.

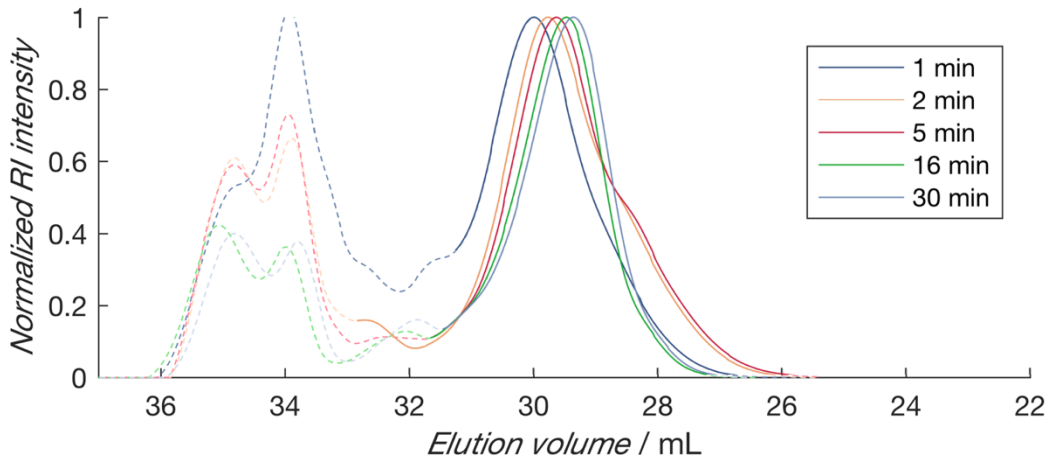

Figure 21: Overlay of elution volume versus normalized intensity of different 2-HEA polymers with varying residence times going from 1 min to 30 min. Polymerization was executed with 1 eq. BiDoPAT and 30 eq. n-BuA in 1,4-dioxane in presence of 0.1 eq. AIBN at 100 °C. The dotted line marks the part of the graph which is considered less important for the polymer.

The peak of the poly(2-HEA) shifts with increasing residence time (Figure 21). However, between 32 mL and 36 mL, there are some lower molecular weights present, from which the one around 35 mL is from the toluene marker in the GPC solvent. The peak around 34 mL could be due to some residual solvent with monomer after the precipitation in hexane. Hexane evaporates relatively easy but placing the poly(2-HEA) under vacuum gave some strange results which are connected with theshoulder present in some graphs, clearly visible in the plot of 2 min and 5 min (Figure 21).

Further investigation showed that the shoulder manifests itself over time (Figure 22, Yellow). After addition of tributylphosphine (TBP) to the GPC vial and remeasuring the same sample again, the shoulder disappears (Figure 22, Red). However, unclear of what has formed and how it has formed, the formation of disulphides over time could be the cause of this shoulder since phosphorous nucleophiles such as TBP reduce disulphides[31].

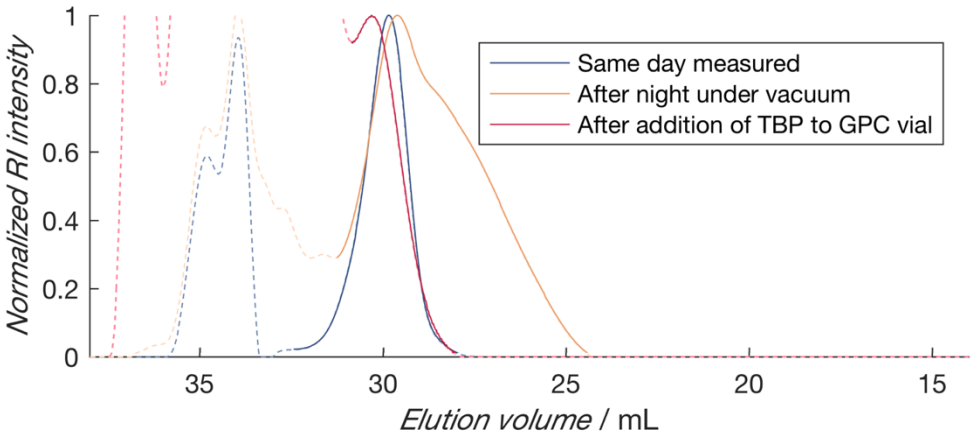

Figure 22: Overlay of elution volume versus normalized intensity of a 2-HEA polymer directly after polymerization, after a night under the vacuum and after addition of TBP to the GPC vial. The dotted line marks the part of the graph which is considered less important for the polymer.

When adding the TBP to the GPC vial, it resulted in a relative strong concentration of TBP, explaining why the graph of the elution volume after adding TBP has such a predominant peak at 33 mL. Since RAFT groups are expected to be intact, the fact that TBP can reduce the shoulder is an unexpected and not directly explicable result. The shoulder appears to a lesser extent when the polymer has been stored in the freezer. For this reason, poly(2-HEA) was always modified as soon as possible after the polymerization or directly stored. Interestingly, the manifestation of the shoulder did not happen with poly(*n*-BuA), despite undergoing vacuum and storage for a longer period at room temperature.

The conversion of the polymers increased with increasing residence time. The molecular weight was also determined by ^{1}H NMR, symbolized by $M_{n,\ 1H\ NMR}$, and plotted against the conversion (Figure 23). Since the M_n of the GPC output was not reliable, it was determined by ^{1}H NMR. From the conversion, the $\ln([M]_0/[M]_t)$ was determined and plotted against the time (Figure 36) (Appendix, Table 3).

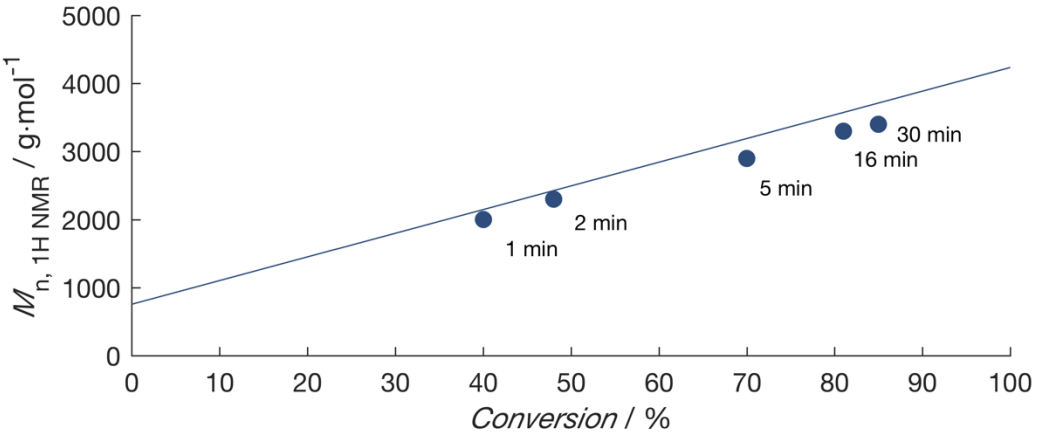

Figure 23: M_n determined by ^{1}H NMR plotted against the conversion of different 2-HEA polymers with varying residence times going from 1 min to 30 min. Polymerization was executed with 0.1 eq AIBN, 1 eq. BiDoPAT and 30 eq. 2-HEA in 1,4-dioxane at 100 °C. For the molecular weight distribution, a theoretical line determined and plotted with the GPC output

In the $M_{n,\ 1H\ NMR}$ versus conversion plot for the poly(2-HEA), the theoretical linear correlation corresponds well with the determined molecular weights (Figure 23). The determined $M_{n,\ 1H\ NMR}$ values correspond well with the theoretical $M_{n,\ 1H\ NMR}$ (Figure 23, line). When comparing the $M_{n,\ 1H\ NMR}$ values of the poly(2-HEA) to the $M_{n,\ 1H\ NMR}$ values of poly(*n*-BuA) with the same residence time, the reaction is slower. Since the used 2-HEA concentration is lower than the used *n*-BuA concentration, a slower reaction time can be expected.

The relationship between the $\ln([M]_0/[M]_t)$ and the time stagnates at 16 min, corresponding with a conversion of 64% and a $M_{n,\ 1H\ NMR}$ of 2500 g·mol^{-1}.

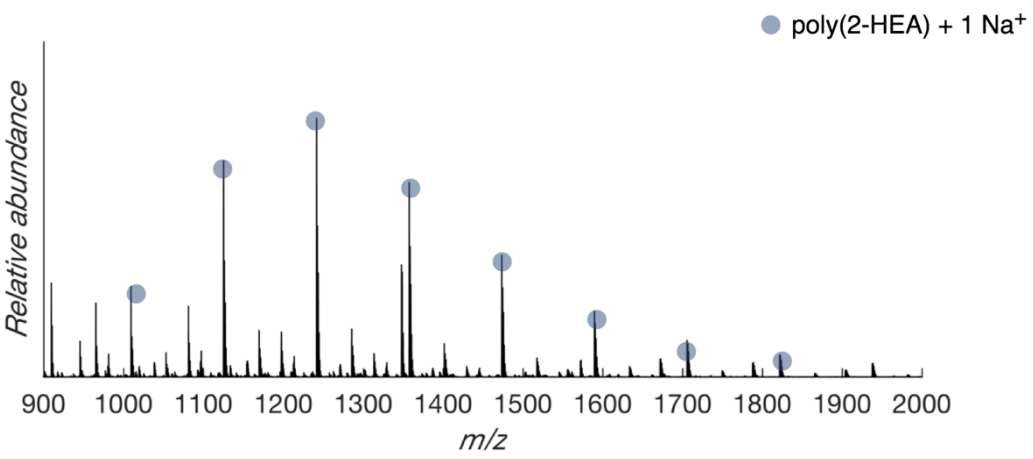

Figure 24: ESI-MS for single charged poly(2-HEA). Polymerization was executed with 1 eq. BiDoPAT and 30 eq. 2-HEA in 1,4-dioxane in presence of 0.1 eq. AIBN at 100 °C (blue).

The main peaks in the ESI-MS spectrum match the molecular mass of the poly(2-HEA) (Figure 24). The ionization of the poly(2-HEA) polymer seemed rather difficult, which is why the noise is relatively high. Further modification is thus possible since the RAFT-groups are present. Depending on the application, a different M_n can be chosen. The poly(2-HEA) modification was executed *in situ* since separate steps would increase the risk of undesired side reactions.

As first modification experiment, a thiol-ene click reaction was executed with 5 eq. hexylamine and 10 eq. HDDA (Figure 25).

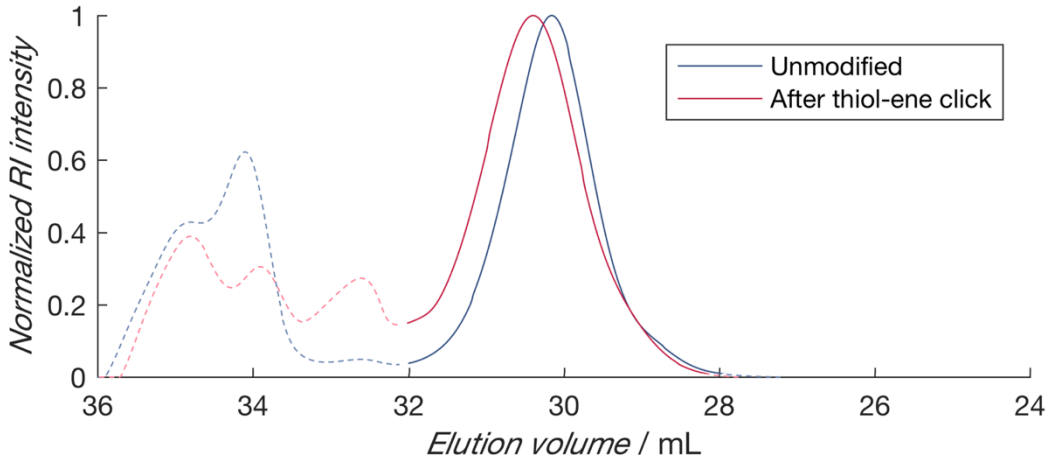

Figure 25: Molecular weight distribution of poly(2-HEA) before modification (blue) and after the thiol-ene click reaction (red) whereby 5 eq. hexylamine and 10 eq. HDDA were used. The dotted line marks the part of the graph which is considered less important for the polymer.

The elution volume indicates that the modified polymer (Figure 25, Red) is slightly shifted towards a higher elution volume, and thus a lower M_n, which might indicate the presence of some unwanted side products. The ESI-MS confirms the presence of side product and indicates that the reaction was not completely successful (Figure 26). A repetition of the experiment with the lower amount of hexylamine (5 eq.) and HDDA (10 eq.) gave the similar results.

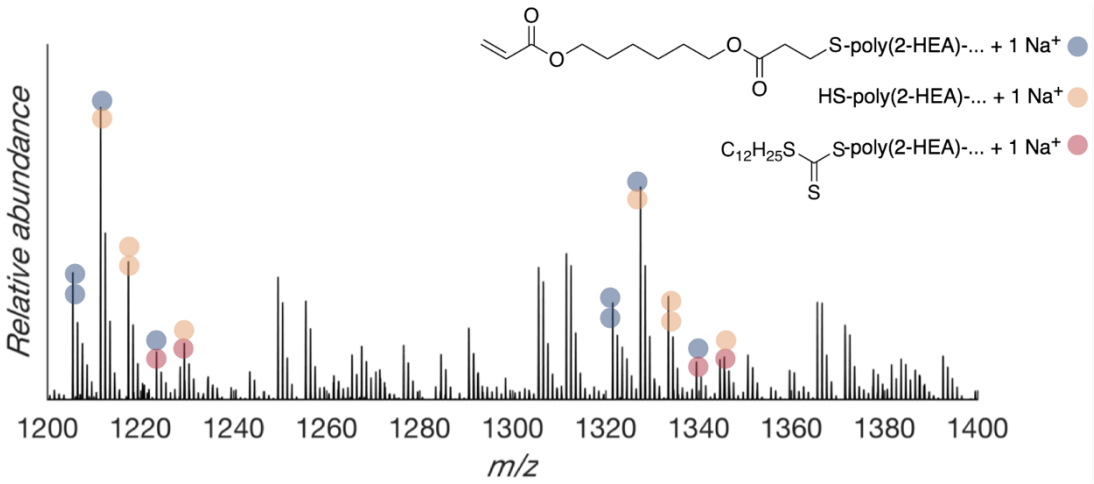

Figure 26: ESI-MS for modified poly(2-HEA) whereby 5 eq. hexylamine and 10 eq. HDDA were used. The two circles represent the end group functionalities from one polymer chain, whereby blue the HDDA, yellow a thiol and red the RAFT agent.

Several absolute weight distributions can be found in the ESI-MS indicating that there is a mixture of polymers whereby the two end groups are a combination of unreacted RAFT agents, thiol-groups or successfully reacted species. To roughly estimate how much unreacted RAFT groups were left, an UV-Vis spectrum was measured (Appendix, Figure 37). Since the RAFT agent had an absorbance around 360 nm, the maxima of these peaks from before and after the thiol-ene reaction were used to determine the ratio of unreacted RAFT-agent in the polymer sample. Thus, for the reaction that was executed with 5 eq. hexylamine and 10 eq. HDDA, there is still around 30% unreacted RAFT agent present in the polymer. For this reason, a second test was executed with a more hexylamine (30 eq.) and HDDA (20 eq.) (Figure 27).

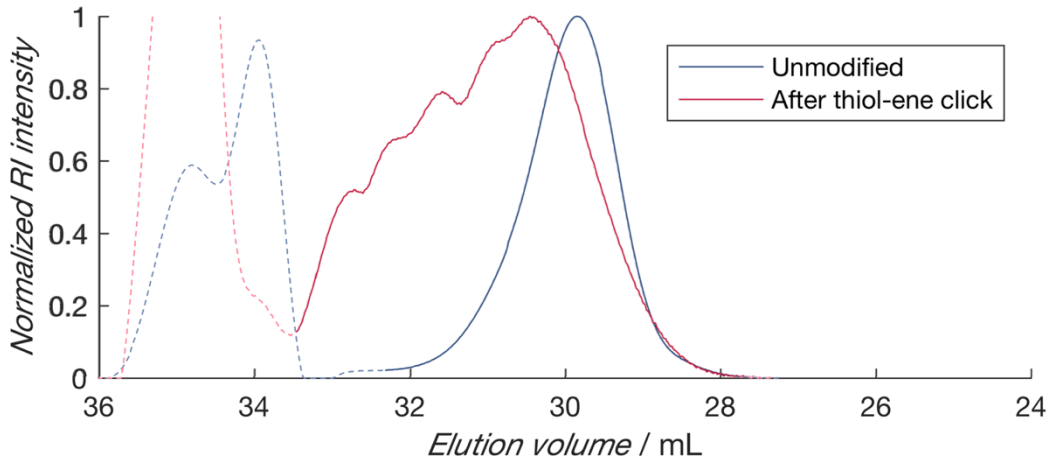

Figure 27: Molecular weight distribution of poly(2-HEA) before modification (blue) and after the thiol-ene click reaction (red) whereby 30 eq. hexylamine and 20 eq. HDDA were used. The dotted line marks the part of the graph which is considered less important for the polymer.

Even though a UV-Vis measurement indicated that there were no unreacted RAFT groups present (Appendix, Figure 38), the GPC overlay indicated that there are side products with low molecular weights (Figure 27, Red). Compared with the M_n from the this is a very unexpected result for which no direct explanation could be given.

Determining what happened proved to be difficult since the polymer did not seem ionize well, which made the ESI-MS very difficult to interpret. A possible solution would be to measure the ESI-MS spectra in negative mode.

Both poly(2-HEA) polymers were tested, despite the 30% RAFT agents that were present in the poly(2-HEA) synthesized with 5 eq. hexylamine. The difference in curing between the two polymers gave unexpected results and will be discussed in the next section.

3.2 Curing

Several resin mixtures were prepared and tested to find the optimal curing conditions. A mixture consisted of polymer, initiator, additional crosslinker and solvent. The solvent was added to make the mixture fit for spincoating. During spincoating, the solvent evaporates leaving a mixture of polymer, initiator and crosslinker onto the surface. The method to calculate the overall amount of crosslinking (Equation 1) is a rough estimation. Detachment of the polymer from the substrate or limitations from the analytic balance can have an influence on the results.

Different exposure times were tested for different energies with pure crosslinker and with a mixture of crosslinker and 5 mol% DMPA (Appendix, Figure 39). In general, one can conclude that there had to be photoinitiator present to trigger the hardening and that 5 $mW \cdot cm^{-2}$ was too low for sufficient curing. 10 $mW \cdot cm^{-2}$ and 15 $mW \cdot cm^{-2}$ did trigger the curing more sufficient and the 15 $mW \cdot cm^{-2}$ was used in all following experiments. The poly(2-HEA) where the UV-Vis indicated that there were no RAFT groups present was tested with an up to 5 mol% initiator concentration and 10 min exposure time. The resin mixture was rinsed off completely after exposure to UV-light. The unexpected GPC result of the could be an indication that something went wrong during the thiol-ene click reaction. A repetition of the thiol-ene click reaction with 30 eq. hexylamine resulted in similar results, with no resin mixture left on the substrate after curing. In contrast, when testing the poly(2-HEA) with 30% RAFT groups, the resin present after rinsing was around 90%. Repeating the thiol-ene click reaction with 5 eq. of hexylamine resulted in the again in 30% unreacted RAFT agent. The reason why the poly(2-HEA) with 30% RAFT groups works better is unclear, but nevertheless this polymer was used in further resin.

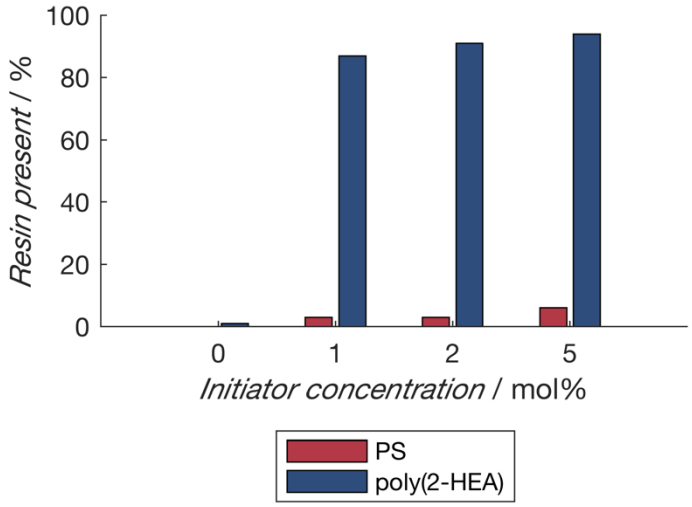

Figure 28: Resin present (%)calculated with equation 1 versus the initiator concentration (mol%) ranging from 0 to 5 for modified PS (red) and poly(2-HEA) (blue).

When comparing the two resins made from different modified polymers, PS and poly(2-HEA), the modified PS cured considerably less well than the modified poly(2-HEA) (

Figure 29). Even with the addition of HDDA to PS, the highest ratio (1:1) with 5 mol% initiator resin only stayed for approximately 20% on the substrate after curing and rinsing (Appendix, Figure 40). The modified poly(2-HEA) resin did significantly better than PS, reaching values of around 90%. A possible explanation could be that at the moment of curing, PS has precipitated which reduces the

efficiency of the curing. A possible solution would be that PS would be spincoated and cured with a less volatile solvent. A second possibility is that when using PS, similar limitations are observed for curing as for photopolymerizations.

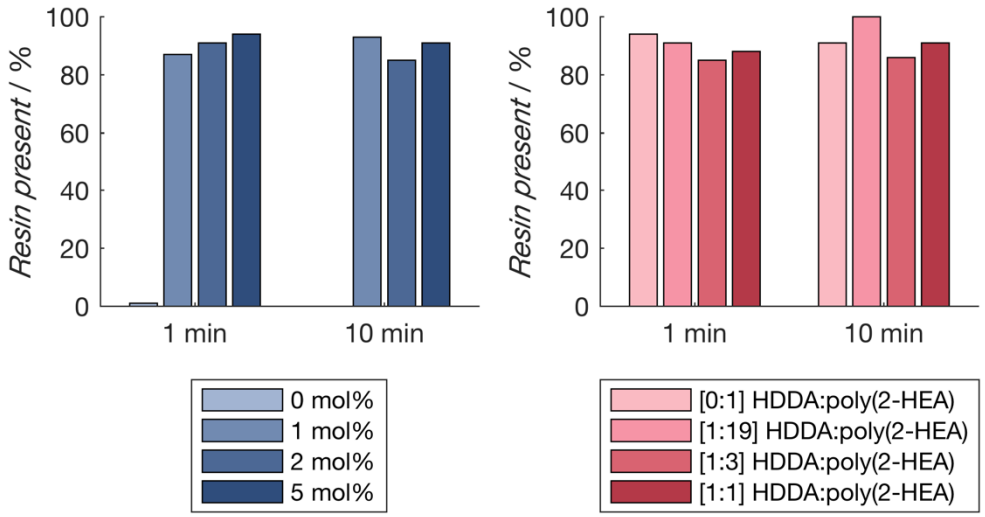

Figure 29: Poly(2-HEA) resin present (%) calculated with equation 1 of samples after rinsing with THF for 1 min and 10 min exposure time. The amount of initiator (blue) and the amount of crosslinker (red) was varied.

The curing of the modified poly(2-HEA) polymer is achieved after 1 min already (Figure 29). The difference in curing between 1 mol% DMPA and 5 mol% DMPA is minimal but the curing process does not work without initiator (Figure 29, Blue). Polymer resins without additional crosslinker worked as well as resins without crosslinker (Figure 29, Red). This given allows us to work with resins purely made from RAFT polymer, which means that most of its properties will be maintained.

3.3 Functionalization of aluminium substrates

Three different particles were used to test the attachment: suspension polymerization NIPs, bulk polymerization nicotine NIPs and bulk polymerization nicotine MIPs. To verify that the particles had indeed free vinyl groups, ATR-IR spectra were measured (Figure 30). The vinyl groups will ensure that the particles are covalently attached to the resin and it is thus important that they are present.

In between the measurements, the crystal was cleaned with absolute ethanol. The shape and size difference between the suspension and bulk polymerization particles was studied with optical microscopy.

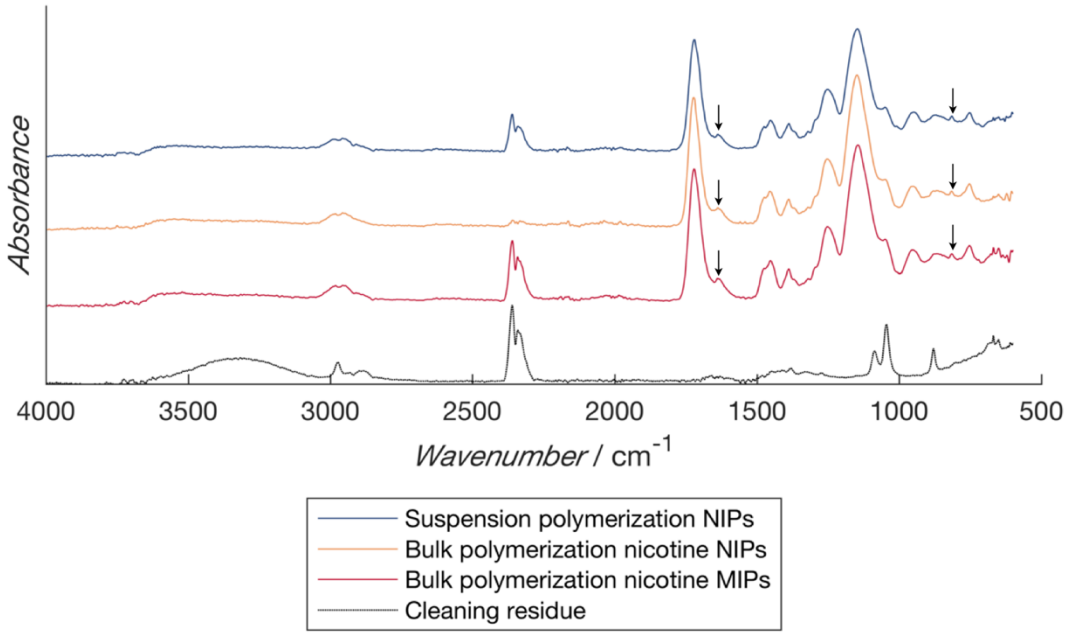

Figure 30: Stacked plot of different ATR-IR spectra from different particles. The peaks at 1635 cm^{-1} (left) and 810 cm^{-1} (right) are indicated by arrows.

An absorbance peak around 1635 cm^{-1} can be assigned to an out of plane bending of C-H on the $RCH=CH_2$ of the vinyl group. Absorbance peaks around 810 cm^{-1} can be due to the stretching vibration of $CH=CH_2$[32]. Both peaks can be assigned to all the ATR-spectra of the three different particles, suggesting that all the particles have indeed vinyl groups present (Figure 30, Arrows). The peaks around 2300 cm^{-1} are most likely an artefact of the ethanol used for cleaning.

The suspension particles are round and approximately the same size: ±40 µm. In contrast, particles made by bulk polymerization have a more crystal-like structure where the size varies from particle to particle.

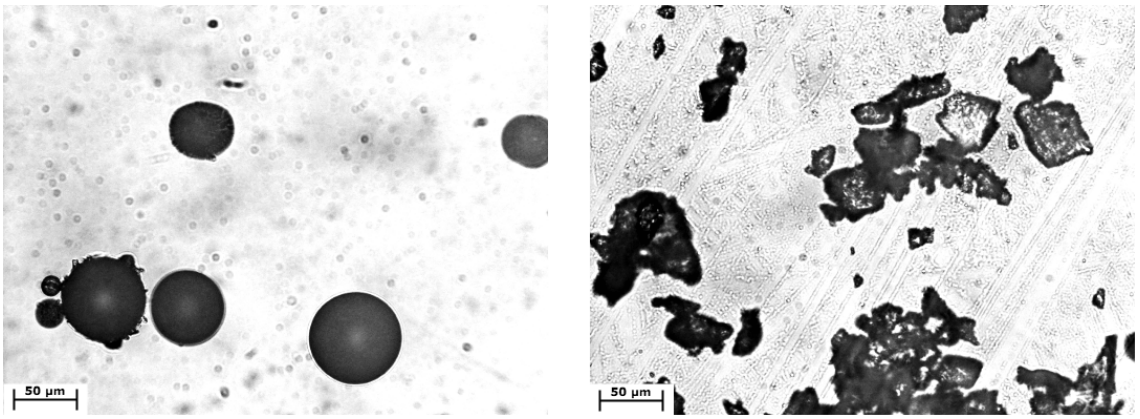

Figure 31: Microscopy pictures from suspension NIPs (left) and bulk NIPs (right).

Since the thickness of the adhesive layer needs to be chosen with the size of the particles in mind, suspension NIPs are more straightforward since their size is approximately the same for all particles. The bulk NIPs have both particles of over 50 µm and small particles of 5 µm, making it a challenge to determine the ideal thickness.

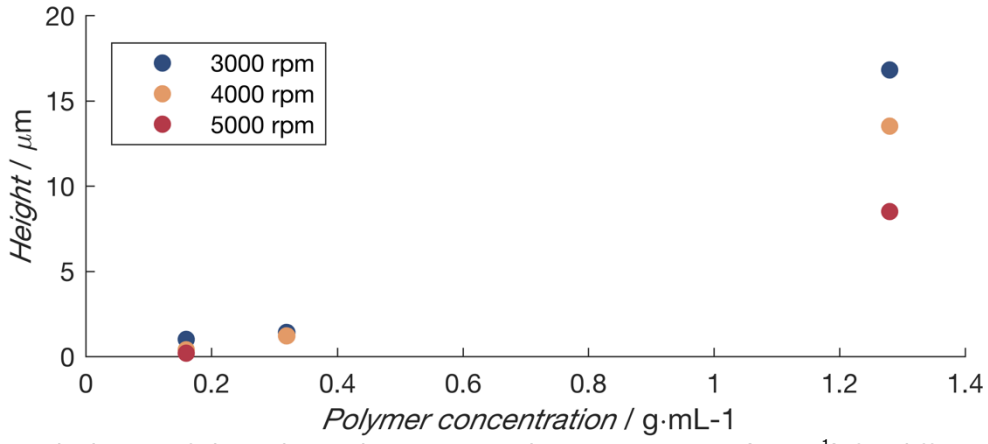

Figure 32: Thickness of the polymer layer versus the concentration ($g \cdot mL^{-1}$) for different spincoat speeds. Polymer resin was dissolved in tetrahydrofuran and spincoated at 3000 rpm (blue), 4000 rpm (yellow) or 5000 rpm (red) at a velocity of 1650 $rmp \cdot s^{-1}$

The adhesive layer was targeted to have a thickness of approximately half the diameter of the MIP particles. First, two parameters that influenced the thickness of the adhesion layer were investigated: the polymer concentration and the speed of the spincoater (Figure 32). The thickness of the adhesive layer can easily be controlled by the concentration of the polymer and the spincoat parameters. Pure polymer was too viscous to successfully dissolve the initiator or spincoat the substrates. The higher the concentration, and thus the higher the viscosity of the resin, the thicker the adhesion layer proved to be. Similarly, a slower spincoat speed also increased the thickness going from with 8.5 µm, 13.5 µm and 16.8 µm with respectively 5000 rpm, 4000 rpm and 3000 rpm.

The adhesive layer was targeted to approximately half the diameter of the MIP particles. To obtain an even higher thickness of around 20 µm, a resin mixture of 1.28 $g \cdot mL^{-1}$ was spincoated at 2000 rpm. For bigger particles, a thicker adhesive layer is necessary. When targeting a layer of around 6 µm, a mixture of 0.5 $g \cdot mL^{-1}$ at 3000 rpm was used.

When functionalizing the aluminium substrates with the suspension NIPs, a layer thickness of around 20 µm was targeted. The substrate was visualized before and after exposure to a demi-water flow by merging several microscope pictures together (Appendix, Figure 42). There is a decrease in NIP particles, most likely due to friction with the O-ring. Two microscopy pictures of the same place in the middle of the substrate revealed that most of the NIP particles stayed in place, but there are still some that are removed after the exposure to flow (Figure 31, Yellow circle).

The visualisation of the airbubbles with the microscope was not performed due technical difficulties with the sensor device and becomes a direct future outlook.

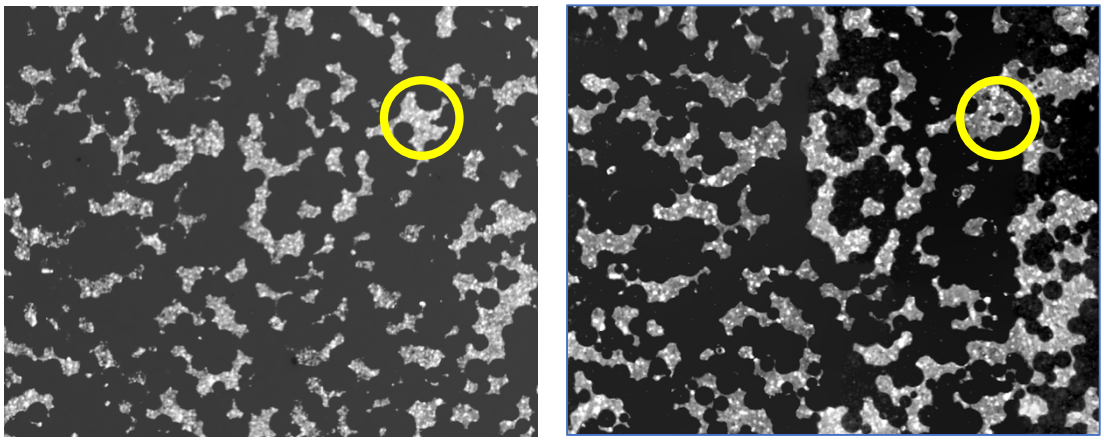

Figure 33: Microscopy pictures of substrate functionalized with suspension NIP particles. The adhesion layer is a poly(2-HEA) resin with 1mol% photoinitiator in THF. The layer thicknes was targeted at 20 µm. The substrate was photographed before (above) and after (below) exposure to demi-water flow. The yellow circle indicates a place where NIP particles came loose.

Since the number of MIPs that remained on the substrate is difficult to quantify with microscope pictures, only a general conclusion can be drawn. As future outlook, the attachment of the MIPs can be monitored with a Quartz Crystal Microbalance (QCM) which changes the mass variation per unit area by measuring the change in frequency of a crystal resonator. If MIP particles would be flushed away during a measurement, the frequency would increase. Similarly, the binding of target molecules to the MIP particles can also be detected, which can be used as control for impedance or HTM measurements.

4 Conclusion and future outlook

As proof of principle, styrene was polymerized in batch and in flow via thermal RAFT and yielded a polymer with a molecular weight of 2100 g·mol^{-1} and a $Đ$ = 1.17. Afterwards, the RAFT end groups of the styrene polymer were modified with HDDA. Unfortunately, a resin mixture with modified PS, HDDA crosslinker and initiator did not seem to cure.

The *n*-BuA polymer was polymerized with both a thermal induced polymerization and a photoiniferter polymerization. The option of photoiniferter is interesting since no additional initiator is used, avoiding distortion of the MIP sensor characterization. For photoiniferter, a conversion of 72% for 120 min residence time was reached, corresponding with 4700 g·mol^{-1} a $Đ$ of 1.27. The polymerization via thermal RAFT initiator yielded a conversion of 88% in 16 min residence time, corresponding to a M_n of 3900 g·mol^{-1} and $Đ$ of 1.32. The dispersity stayed below 1.27. Due to time constrains, the use of n-BuA in a resin was not further optimized and is a direct future outlook.

Since the adhesion layer had to be preferably hydrophilic, it was chosen to further focus on polymers which used the hydrophilic 2-HEA monomer. Since the poly(2-HEA) needed to be synthesized at much lower concentrations, the polymerization was less efficient resulting in a conversion of from 64% for 16 min residence time. The remaining solvent and monomer was removed by precipitating the poly(2-HEA) in hexane.

For the curing assays, after 1 min exposure to UV-light, around 90% of the poly(2-HEA) based resin stayed onto the surface even without additional crosslinker. The photo-initiator concentration was kept 1 mol% to coat the substrates. Lower initiator concentrations can be considered for further optimization. The curing of the PS resin was incomplete and unsatisfactory.

The thickness of the adhesive layer was varied by changing the concentration and the rotational speed of the spincoater. The suspension NIP particles were attached to an aluminium substrate with an adhesive layer of around 20 µm. After curing and exposing the functionalized substrate to a demi-water flow, the particles were mostly attached, with exception to the side of the O-ring due to friction. In the future, the attachment of the MIPs can be monitored with a Quartz Crystal Microbalance (QCM). The decrease in attachment of air bubbles is one of the next tests that should be executed to characterize the resin. Further measurements with the biosensor should confirm if the quality of measurements is consistent or even improved.

Moreover, the successful development of a polymer based resin using RAFT polymerization shows the path towards the production of precisely tuned polymer resins. As control over composition of the polymer and its molecular weight is achieved, these resins can contain specific characteristics. By using RAFT, a vast monomer library is available depending on the needs of possible target applications. Furthermore, from an industrial point of view, we have shown the synthesis of these polymers in a continuous flow process, which allows for relatively easy up-scaling.

References

[1] H. Namazi, *BioImpacts : BI* **2017**, *7*, 73-74.
[2] A. Ambrogelly, S. Palioura, D. Söll, *Nature Chemical Biology* **2006**, *3*, 29.
[3] N. Bhalla, P. Jolly, N. Formisano, P. Estrela, *Essays in Biochemistry* **2016**, *60*, 1-8.
[4] K. Eersels, P. Lieberzeit, P. Wagner, *ACS Sensors* **2016**, *1*, 1171-1187.
[5] E. M. Peck, B. D. Smith, in *Synthetic Receptors for Biomolecules: Design Principles and Applications*, The Royal Society of Chemistry, **2015**, pp. 1-38.
[6] B. van Grinsven, M. Eersels K Fau - Peeters, P. Peeters M Fau - Losada-Perez, T. Losada-Perez P Fau - Vandenryt, T. J. Vandenryt T Fau - Cleij, P. Cleij Tj Fau - Wagner, P. Wagner.
[7] K. Betlem, M. P. Down, C. W. Foster, S. Akthar, K. Eersels, B. van Grinsven, T. J. Cleij, C. E. Banks, M. Peeters, *MRS Advances* **2018**, *3*, 1569-1574.
[8] T. Kamra, S. Chaudhary, C. Xu, L. Montelius, J. Schnadt, L. Ye, *Journal of Colloid and Interface Science* **2016**, *461*, 1-8.
[9] R. Thoelen, R. Vansweevelt, J. Duchateau, F. Horemans, J. D'Haen, L. Lutsen, D. Vanderzande, M. Ameloot, M. vandeVen, T. J. Cleij, P. Wagner, *Biosensors and Bioelectronics* **2008**, *23*, 913-918.
[10] B. van Grinsven, K. Eersels, O. Akkermans, S. Ellermann, A. Kordek, M. Peeters, O. Deschaume, C. Bartic, H. Diliën, E. Steen Redeker, P. Wagner, T. J. Cleij, *ACS Sensors* **2016**, *1*, 1140-1147.
[11] B. Geerets, M. Peeters, B. van Grinsven, K. Bers, W. de Ceuninck, P. Wagner, *Sensors (Basel, Switzerland)* **2013**, *13*, 9148-9159.
[12] S. Tanodekaew, S. Channasanon, P. Uppanan, *Journal of Biomedical Materials Research Part B: Applied Biomaterials* **2013**, *102*, 604-611.
[13] I. M. Garcia, V. C. B. Leitune, F. Visioli, S. M. W. Samuel, F. M. Collares, *Journal of Dentistry* **2018**.
[14] R. B. Grubbs, *Polymer Reviews* **2011**, *51*, 104-137.
[15] J.-S. Wang, K. Matyjaszewski, *Journal of the American Chemical Society* **1995**, *117*, 5614-5615.
[16] J. Chiefari, Y. K. Chong, F. Ercole, J. Krstina, J. Jeffery, T. P. T. Le, R. T. A. Mayadunne, G. F. Meijs, C. L. Moad, G. Moad, E. Rizzardo, S. H. Thang, *Macromolecules* **1998**, *31*, 5559-5562.
[17] E. Hoyle Charles , N. Bowman Christopher *Angewandte Chemie International Edition* **2010**, *49*, 1540-1573.
[18] aB. Wenn, T. Junkers, *Macromolecules* **2016**, *49*, 6888-6895; bX. Pan, M. A. Tasdelen, J. Laun, T. Junkers, Y. Yagci, K. Matyjaszewski, *Progress in Polymer Science* **2016**, *62*, 73-125.
[19] C. Song, S. Yu, C. Liu, Y. Deng, Y. Xu, X. Chen, L. Dai, *Materials science & engineering. C, Materials for biological applications* **2016**, *62*, 45-52.
[20] Z.-Q. Jiang, S.-Q. Zhao, Y.-X. Su, N. Liu, Z.-Q. Wu, *Macromolecules* **2018**, *51*, 737-745.
[21] A. Tochwin, A. El-Betany, H. Tai, K. Chan, C. Blackburn, W. Wang, *Polymers* **2017**, *9*, 443.
[22] G. Zeng, M. Liu, R. Jiang, Q. Huang, L. Huang, Q. Wan, Y. Dai, Y. Wen, X. Zhang, Y. Wei, *Materials science & engineering. C, Materials for biological applications* **2018**, *83*, 154-159.
[23] G. Moad, E. Rizzardo, H. Thang San, *Polymer International* **2010**, *60*, 9-25.
[24] C. Boyer, A. Granville, P. Davis Thomas, V. Bulmus, *Journal of Polymer Science Part A: Polymer Chemistry* **2009**, *47*, 3773-3794.
[25] aG.-Z. Li, R. K. Randev, A. H. Soeriyadi, G. Rees, C. Boyer, Z. Tong, T. P. Davis, C. R. Becer, D. M. Haddleton, *Polymer Chemistry* **2010**, *1*, 1196-1204; bJ. W. Chan, C. E. Hoyle, A. B. Lowe, M. Bowman, *Macromolecules* **2010**, *43*, 6381-6388.
[26] G. Moad, E. Rizzardo, S. H. Thang, *Australian Journal of Chemistry* **2012**, *65*, 985-1076.
[27] J. Vandenbergh, G. Ramakers, L. van Lokeren, G. van Assche, T. Junkers, *RSC Advances* **2015**, *5*, 81920-81932.
[28] T. Junkers, *Macromolecular Chemistry and Physics* **2016**, *218*, 1600421.
[29] E. Baeten, J. J. Haven, T. Junkers, *Polymer Chemistry* **2017**, *8*, 3815-3824.
[30] E. Vargün, A. Usanmaz, *Journal of Polymer Science Part A: Polymer Chemistry* **2005**, *43*, 3957-3965.
[31] O. Dmitrenko, C. Thorpe, R. D. Bach, *The Journal of organic chemistry* **2007**, *72*, 8298-8307; bR. E. Humphrey, J. L. Potter, *Analytical Chemistry* **1965**, *37*, 164-165.
[32] T. Hong Bong, S. Shin Kwon, S. Kim Dae, *Journal of Applied Polymer Science* **2005**, *98*, 1180-1185.

Appendix

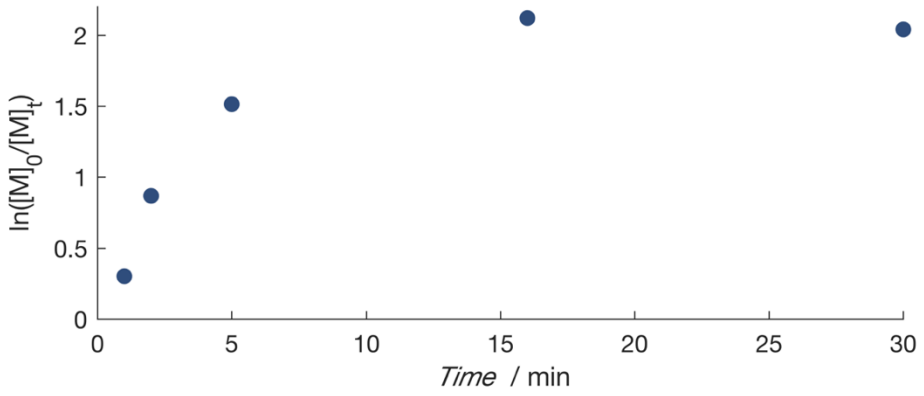

Figure 34: $\ln([M]_0/[M]_t)$ versus time plot for *n*-BuA polymerized with BiDoPAT for different residence times. Polymerization was executed with 1 eq. BiDoPAT and 30 eq. n-BuA in 1,4-dioxane in presence of 0.1 eq. AIBN at 100 °C.

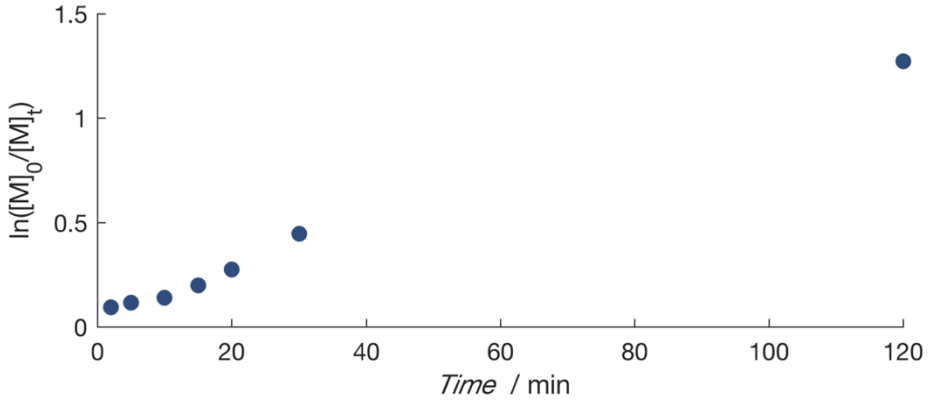

Figure 35: $\ln([M]_0/[M]_t)$ versus time plot for *n*-BuA polymerized with BiDoPAT for different residence times. Polymerization was executed with 1 eq. BiDoPAT and 40 eq. *n*-BuA in butyl acetate under UV light.

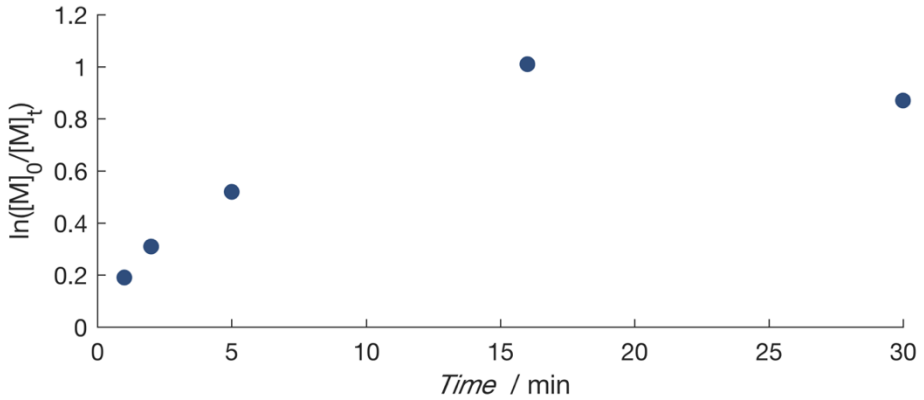

Figure 36: $\ln([M]_0/[M]_t)$ versus time plot for 2-HEA polymerized with BiDoPAT for different residence times. Polymerization was executed with 1 eq. BiDoPAT and 30 eq. 2-HEA in 1,4-dioxane in presence of 0.1 eq. AIBN at 100 °C.

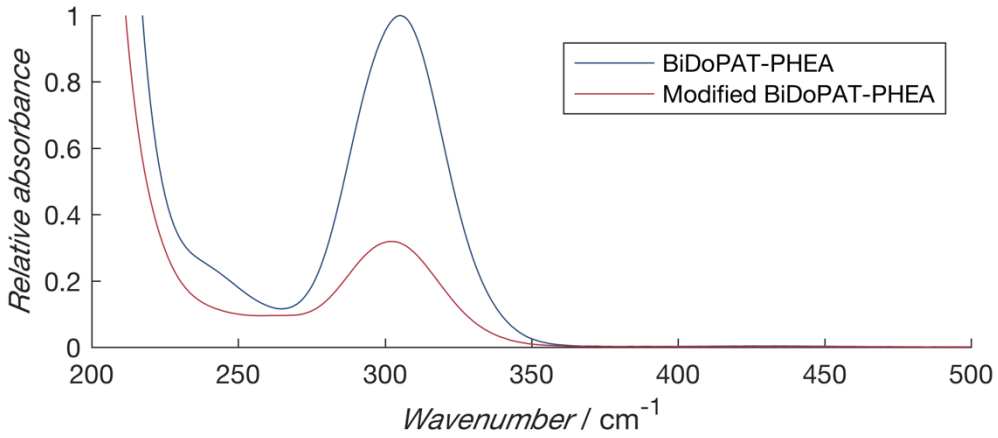

Figure 37: Uv-vis spectra from poly(2-HEA) before modification (blue) and after modification with 5 eq. hexylamine and 10 eq. HDDA (red).

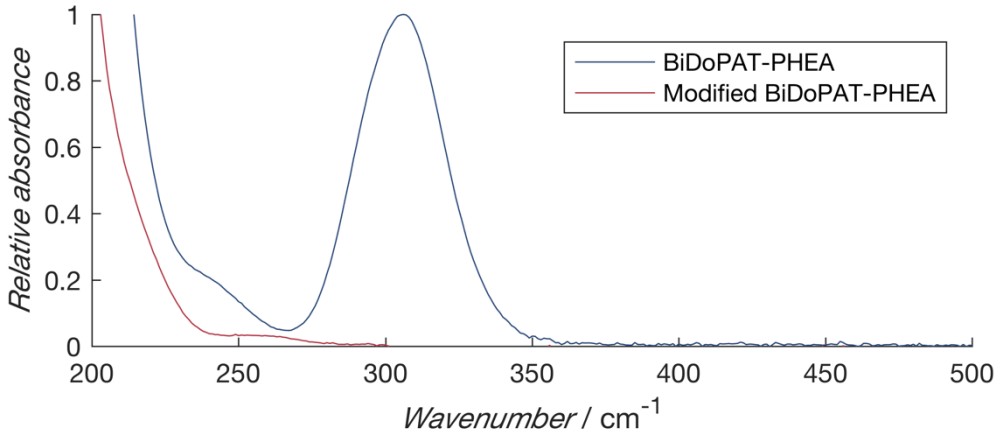

Figure 38: Uv-vis spectra from poly(2-HEA) before modification (blue) and after modification with 30 eq. hexylamine and 20 eq. HDDA (red).

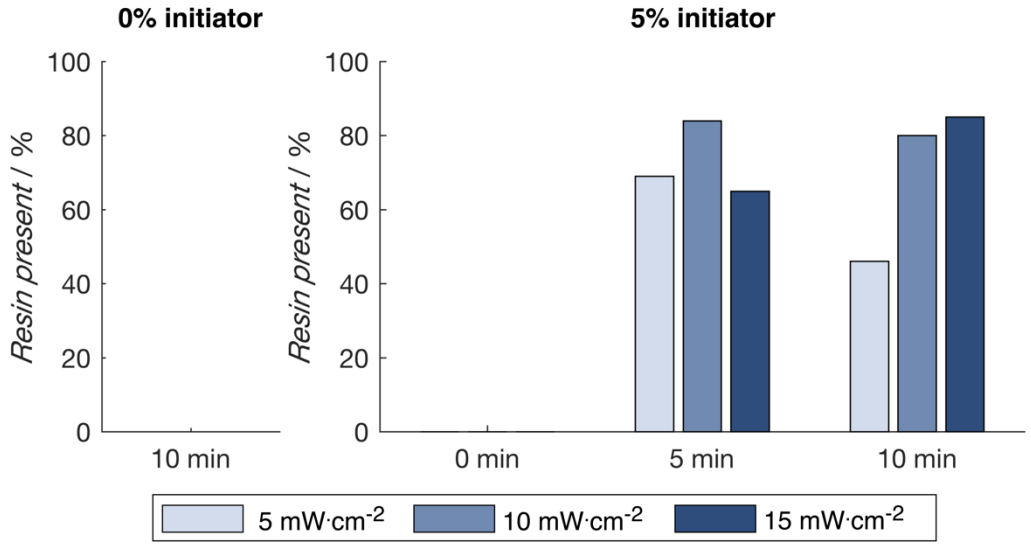

Figure 39: Poly(2-HEA) resin present (%) calculated with equation 1 of samples after rinsing with THF for no initiator (left) or for 5 mol% initiator (right) and no initiator (left). Samples were exposed to UV-light for 0 min, 5 min or 30 min.

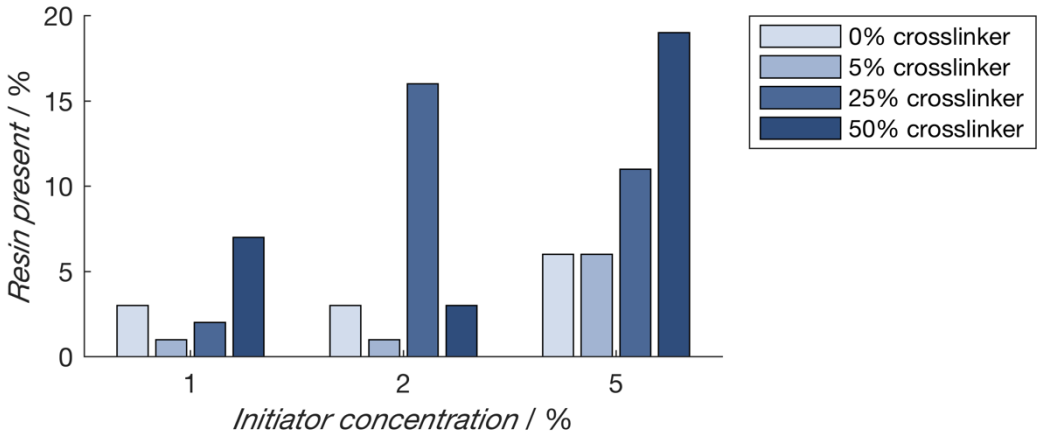

Figure 40: PS resin present (%) calculated with equation 1 of samples after rinsing with THF for 5 mol% initiator (right) and no initiator (left). Samples were exposed to UV-light for 0 min, 5 min or 30 min.

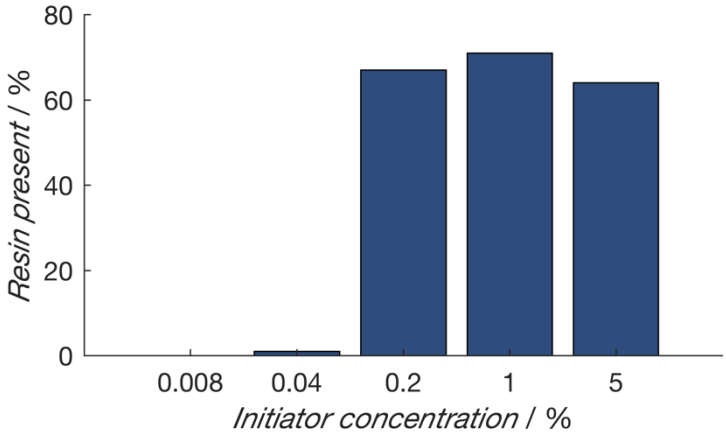

Figure 41: Poly(2-HEA) resin present (%) calculated with equation 1 of samples after rinsing with THF with different initiator concentrations (mol%)

Table 1: TI nBuA

Residence time / min	Conversion / %	M_n / g·mol^{-1}	Dispersity	$\ln([M]_0/[M]_t)$
1	26	1900	1.20	0.30
2	58	2600	1.21	0.87
5	78	3500	1.27	1.51
16	88	3900	1.32	2.12
30	87	3500	1.27	2.04

Table 2: PI nBuA

Residence time / min	Conversion / %	M_n / g·mol^{-1}	Dispersity	$\ln([M]_0/[M]_t)$
2	9	1000	1.10	0.09
5	11	1100	1.13	0.12
10	13	1300	1.18	0.14
15	18	1500	1.22	0.20
20	24	2300	1.27	0.27
30	36	2600	1.15	0.45
120	72	4700	1.27	1.27

Table 3: TI nBuA

Residence time / min	Conversion / %	M_n / g·mol^{-1}	Dispersity	$\ln([M]_0/[M]_t)$
1	17	1300	-	0.19
2	26	1600	-	0.31
5	42	1800	-	0.52
16	64	2500	-	1.01
30	58	2500	-	0.87

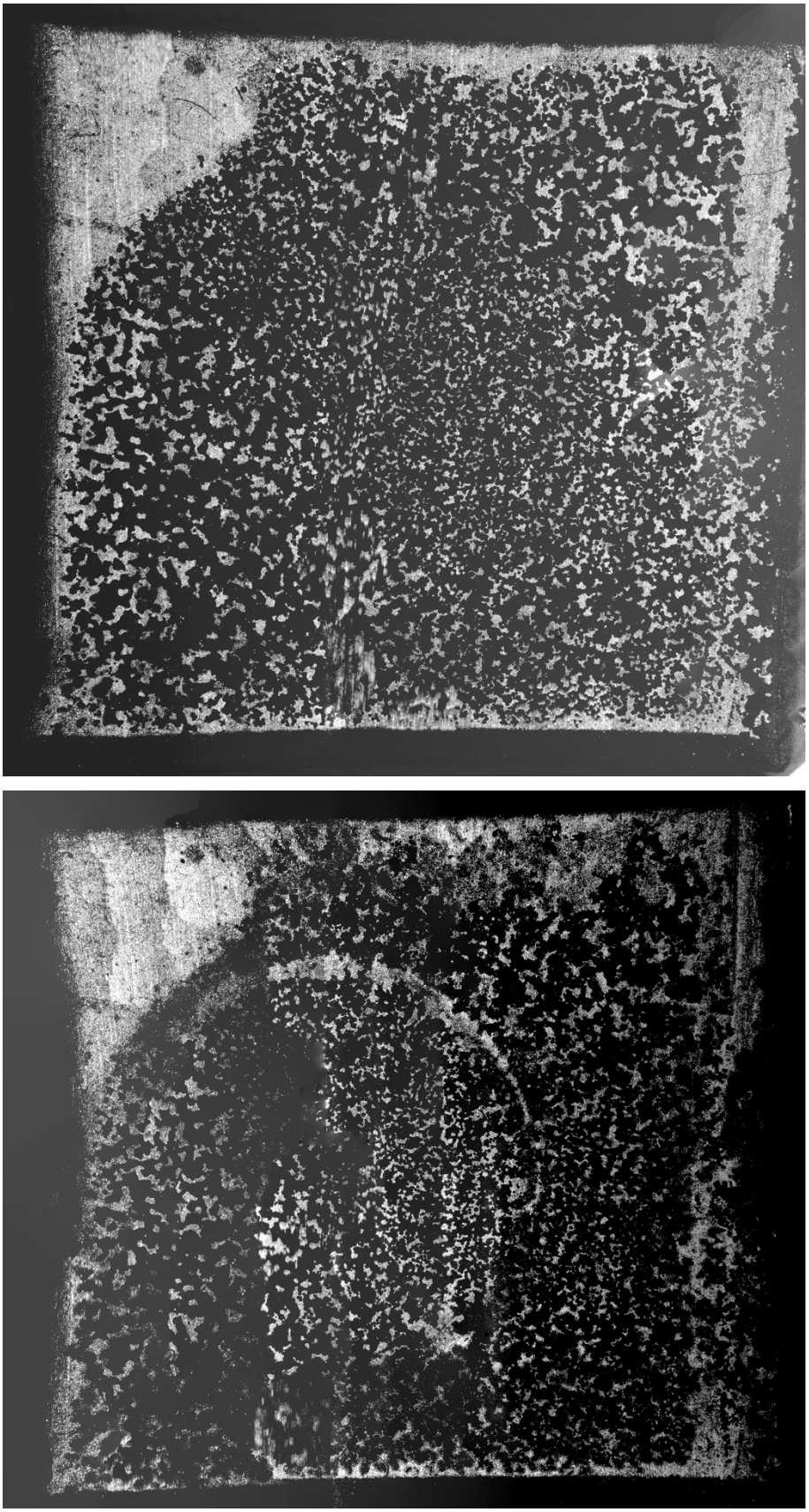

Figure 42: Merged microscopy pictures of substrate functionalized with suspension NIP particles. The adhesion layer is a poly(2-HEA) resin with 1mol% photoinitiator in THF. The layer thicknes was targeted at 20 µm. The substrate was photographed before (above) and after (below) exposure to demi-water flow.

Auteursrechtelijke overeenkomst

Ik/wij verlenen het wereldwijde auteursrecht voor de ingediende eindverhandeling:
**Development of a polymer resin as an improved adhesion layer in molecularly imprinted polymer based biosensors
**

Richting: **Master of Biomedical Sciences-Bioelectronics and Nanotechnology**
Jaar: **2018**

in alle mogelijke mediaformaten, - bestaande en in de toekomst te ontwikkelen - , aan de Universiteit Hasselt.

Niet tegenstaand deze toekenning van het auteursrecht aan de Universiteit Hasselt behoud ik als auteur het recht om de eindverhandeling, - in zijn geheel of gedeeltelijk -, vrij te reproduceren, (her)publiceren of distribueren zonder de toelating te moeten verkrijgen van de Universiteit Hasselt.

Ik bevestig dat de eindverhandeling mijn origineel werk is, en dat ik het recht heb om de rechten te verlenen die in deze overeenkomst worden beschreven. Ik verklaar tevens dat de eindverhandeling, naar mijn weten, het auteursrecht van anderen niet overtreedt.

Ik verklaar tevens dat ik voor het materiaal in de eindverhandeling dat beschermd wordt door het auteursrecht, de nodige toelatingen heb verkregen zodat ik deze ook aan de Universiteit Hasselt kan overdragen en dat dit duidelijk in de tekst en inhoud van de eindverhandeling werd genotificeerd.

Universiteit Hasselt zal mij als auteur(s) van de eindverhandeling identificeren en zal geen wijzigingen aanbrengen aan de eindverhandeling, uitgezonderd deze toegelaten door deze overeenkomst.

Voor akkoord,

Van de Reydt, Emma

Datum: **7/06/2018**